Authors' response document

Reconstructing volcanic plume evolution integrating satellite and ground-based data: Application to the 23rd November 2013 Etna eruption

Matthieu Poret, Stefano Corradini, Luca Merucci, Antonio Costa, Daniele Andronico, Mario Montopoli, Gianfranco Vulpiani, and Valentin Freret-Lorgeril

Comments from Larry Mastin (Referee 1)

Main comments

This paper combines deposit mass load data, radar data, and satellite data to reconstruct the grain-size distribution of erupted material from the 23rd November 2013 paroxysmal eruption of Etna volcano, Italy. Reconstruction of grain-size distributions during eruptions is important for modelling and forecasting tephra hazards. But it is laborious, requiring systematic sampling of a tephra deposit and integrating grain-size data. Grain-size data collected from a tephra deposit is also incomplete, because a significant (and usually unknown) fraction of the erupted mass drifts downwind, to distances far beyond the mapped deposit. Few studies have attempted to estimate the fraction of the deposit escapes the mapped area. Yet it is a key input in ash-cloud models used for aviation safety. This is one of very few studies that integrates deposit, radar, and ash-cloud data to derive a complete grain-size distribution (TGSD). For this reason, I support its publication. However, before recommending publication I think it requires significant revision. In particular:

1. Explanations are too long, complicated, and frequently unclear. Many examples are flagged in the accompanying pdf. The revised manuscript should be reviewed again to ensure that it can be understood.

The manuscript was modified keeping in mind the necessity to improve the clarity of the explanations. We hope the revised manuscript is easier to understand.

2. Much of the methodology is not clearly explained. Or at least I head trouble following it. Key issues are:

a. One or more tables should be added summarizing inputs, including model domain, nodal spacing, etc.

We added a table (now Table 2) to report the input parameters with the corresponding ranges. Also, we added an Appendix to summarize the parameterization used for the simulations under the 2 different meteorological databases.

b. There should more explanation (perhaps in a table) of which parameters are changed in each simulation, and how they are changed. In Table 2 for example, I had assumed that the only parameters changed from one row to the next were the relative percentages of the deposit-based TGSD and the radar-based TGSD. But it appears that the total erupted mass is also changing. Why? Is the mass being adjusted to optimize the fit? Does each TGSD have an erupted mass associated with it?

We modified the text in p.7 – lines 12-16 to precise which parameters were modified in each simulation. We also added a table (now Table 2) to report the input parameters with their ranges. The Integrated TGSD was inverted by comparing each tested weighting average combination. For that reason, we reported in Table 3 the best simulations (i.e. optimal α and β*) for all the combinations selected on the basis of the goodness-of-fit procedure (i.e. K ≈ 1), explaining the resulting different TEM estimations. The latter point was described in p.9 – lines 36-39.*

c. Section 3.1 should more fully explain how the radar retrievals are combined to give a TGSD. The radar returns a reflectivity (which can be turned into GSD) for each volume, delineated by horizontal angle, vertical angle, range, and time. How are these combined to give a TGSD for the entire eruption?

Thank you for having pointed out the lack of information. Actually, we considered a spatial and temporal average of the X-Radar-based GSD (referred as PSD: particle size distribution in the main text) to obtain the TGSD for the whole event. The average takes in input each PSD estimated from each single radar resolution volume delineated by horizontal angle, vertical angle, and range distance at each available time step. We modified the text in p.5 – lines 1-13.

d. Section 3.2 should clarify how FPlume output feeds into FALL3D. A list of inputs for FPlume, and another list of its outputs that go into FALL3D, would be helpful.

Thank you for having pointed out the issue. We clarified the section (p.5 – lines 33-41) to better explain how FPlume and FALL3D work together. Additionally, we added a table (now Table 2) to show the key input parameters.

e. Please explain the Poret et al. (2017) method of inverting for alpha and beta (p. 6, line 12). Do you hold plume height and eruption rate constant (using independent information) and then optimize alpha and beta? What range of alpha and beta do you start with before you optimize? Your resulting values, 0.06-0.15 for alpha and 0.2 to 1.0 for beta, are so broad that I'm not sure the inversion is worth including.

Section 3.3 was modified to better describe the inversion procedure, especially for α and β. As mentioned in p.7 – lines 12-16, we hold the column height and inverted α and β following the goodness-of-fit procedure (i.e. RMSEs, K, k ...). The resulting ranges are broad but are regardless to the weighting average combination. The α and β values obtained after inversion for each weighting average combination were added in Table 3 and reported in P.9 – lines 5-7.

f. What factor(s) determine the vertical distribution of mass with height in the FALL3D model? Is this an output from FPlume, or do you use some parameterization, like a Suzuki curve?

We did not use Suzuki's parameterization. In fact, we used the FPlume model to determine the vertical mass distribution. The model uses the air mixing entrainment coefficients (i.e. α and β*) to distribute vertically the mass (Folch et al., 2016). We modified p.5 – lines 33-41 to clarify how FPlume feeds FALL3D.*

3. It would be of great value to discuss some results in the context of other studies. Most significant (in my opinion) is your finding that the mass fraction of fine ash (PM_{20}) is 3.6-9.0 wt% of the erupted mass. This fraction is a critical input into ash-cloud models used for aviation safety because it is the mass that

goes into the downwind cloud. Few studies have constrained it. NOAA's Hysplit model assumes for example that 5% of the erupted mass makes it into the downwind cloud and uses this 5% as model input. At Spurr in 1992, Wen and Rose [1994] estimated about 2% of the erupted mass went into the distal cloud. At Eyja, the estimates range from ~0.9% to 11% [Bonadonna et al., 2011; Dacre et al., 2011; Devenish et al., 2012]. Basaltic eruptions like Etna tend to be very poor in fine ash, hence I would expect a lower fraction. But your 3.6-9 wt% are in the middle of the previous numbers. Does this mean that we don't need to adjust downward when modelling a basaltic eruption? Additional comments are below, and in the attached pdf. Some duplicate points made above. Overall, I think the paper merits publication. But it should be revised to shorten, clarify, improve readability, and explain methods. I look forward to seeing the final version.

Probably there was a misunderstanding on this point. These eruptions are not comparable among them as the fraction of fine ash is very different from one case to the other. It can range from 50% to a few %. The fact that Hysplit or other model assume fraction of about 5% is not related with what we estimate for the Etna eruption. In the former case, 5% would represent the fine ash fraction that escape to aggregation processes and travel far away. In the case of basaltic eruptions fine ash content is lower and hence aggregation less efficient, implying that almost all the fine ash fraction can be transported distally. In the revised version we briefly discussed this point (p.10 – lines 40-42 – p.11 – lines 1-12).

Specific comments

Page 3, line 16, and Figure 2: Is there any evidence that the existence of a whitish plume on top and grayish below was persistent during the eruption? Or is this photo just recording a transient phenomenon? Also, the upper cloud looks light gray to me, not exactly white, like the one in the lower right of Fig. 2.

The plume was observed by cameras from the INGV-OE through visible images that showed the 2 plumes, the greyish above the brownish one. We understood the confusion about the colour name. We replaced "whitish" by "greyish" (p.3 – line 8).

p. 3, line 26. What method(s) does the CAMSIZER use for grain-size analysis? Laser? Settling rates? Some combination?

The CAMSIZER measure optically the grain-size, which was mentioned in p.3 – line 17.

Section 2.1 (page 3): The number of samples collected (7) is pretty small. Thus, there is a strong chance of bias in your results. Can describe where the samples were taken relative to the dispersal axis, and how (or whether) you know the overall distribution of the deposit?

Although a set of 7 samples is a relatively small number, we used the field data as a starting point from which we added radar and satellite data. Moreover, such a small number of samples is common for Etna eruptions. The study does not assume the samples are located within the main axis of the plume, but compares the simulation outputs with the field data, best-fitting the sampled tephra loadings. We do not know the overall distribution, but we based this study on reproducing the field measurements together with the airborne ash observations. In addition, the field-derived TEM is compared to the FALL3D results. We believe that the synergic use of these points increases the relevance of our findings.

p. 3, lines 31-32: The MER estimate of 4.5e06 kg/s for the climax phase comes from the mapped deposit and observed duration. Where does the estimate of 1e06 kg/s come from?

In p.3 – line 23, the MER = 4.5 ± 3.6 × 10^5 kg/s comes from the estimation made in Andronico et al. (2015) and refers to the entire paroxysm (~50 min). The value of 10^6 kg/s concerns the maxima reached during the climax phase (i.e. from 09:55 to 10:14; ~19 min) and comes from Donnadieu et al. (2017).

p. 4, line 21. How do you derive a mass eruption rate from radar? From plume height using FPlume?

In p.4 – line 12, Corradini et al. (2016) reported the total erupted mass not the mass eruption rate. In this study, we have not used the radar data to derive the MER.

p. 4, lines 23-24. I'm getting a little confused about the release of the ice and ash clouds. On p. 3, you seemed to imply that ash and moisture (forming the ice cloud) were released at the same time but at different elevations. Here you seem to be saying that they came out at different times (but maybe overlapped in time).

In p.3 – lines 39-41 – p.4 – lines 1-8, we described the satellite retrievals in terms of mass. We mentioned that ash dominates first in mass, and then ice (produced from the release of water vapour). In Fig. 4, the time discrepancy between ash and ice mass peaks is due to the release of the water vapour coupled with the required time to produce ice from water vapour. To avoid confusion, we clarified the point (p.4 – lines 5-6).

p. 4, lines 10-28. This paragraph needs to be reorganized and reworded to improve its coherence.

The confusing paragraph was reworded and reorganized in 2 paragraphs to gain in clarity helping the reader to follows the flow (p.3 – lines 38-41 – p.4 – lines 1-15).

Equation 1: Does this equation assume that the plane of the block's trajectory is the same as that of the radar beam? If not, I don't see how that the angle between the two is considered. Also, why is ejection velocity important in this study? It is not really related to column height, or MER. Is it just a qualitative indicator of eruption intensity?

Equation 1 is used to calculate the ejection velocity from the near-source detection retrievals of the L-band radar. The equation assumes that block's trajectory is vertical, which is considered by means of the elevation angle of the radar beam ($\theta = 14.9°$). Regarding the use of the ejection velocity data (VOLDORAD 2B), we worked on discretizing the eruption into several phases to best fit the column height observations. From a numerical point of view, we described a phase by a time interval, a column height value, and an average ejection velocity.

P. 5, lines 8-15. This explanation should be reworded to be clearer and more concise. I don't have specific suggestions. But I think you are saying that the field TGSD will be biased toward coarse ash, and that the radar will help constrain the mass of fine ash.

The explanation was corrected trying to be clearer and concise as suggested (p.4 – lines 35-40 – p.5 – line 1). The main point was to mention that the field-derived TGSD cannot represent the

full size-spectrum TGSD and needs to be improved prior use within the FPlume and FALL3D models.

p. 5, lines 19-29. You talk about estimating TGSD from the radar. So, you estimate two independent TGSD's? One from the deposit and another from radar? Perhaps this should be mentioned. It is not clear to me how you derive a TGSD.

The paragraph was unclear and was modified to mention clearly and concisely the estimation of the TGSD from the field measurements (p.4 – lines 35-40) and the X-Radar retrievals (p.5 – lines 1-13).

Section 3.1 (p. 5). There is some critical information I don't see in the explanation of TGSD derived from radar. I assume that the radar provides a TGSD for each volume, delineated by range, and horizontal and vertical angles, and time of the scan. Somehow these volumes are integrated to get a radar-based TGSD for the entire airborne mass. How is this done?

As mentioned above, we considered a spatial and temporal average of the X-Radar-based GSD (referred as PSD: particle size distribution in the main text) to obtain the TGSD for the whole event. The average takes in input each PSD estimated from each single radar resolution volume delineated by horizontal angle, vertical angle, and range distance at each available time step. We modified the text in p.5 – lines 1-13.

p. 5, lines 27-28: "To [integrate the radar and field TGSDs], we investigated the weights at regular intervals until we best-fit the field measurements maintaining the shape of the radar TGSD on the proper grain-size interval". After reading this sentence a couple of times, I'm still not sure exactly how you arrived at a best fit. You adjusted the relative amounts of radar ash and field ash until the heights of the histogram bars in the overlapping interval agreed?

The sentence was confusing. We modified the sentence with the previous ones to better explain the procedure used for estimating the Integrated TGSD (p.5 – lines 14-20). Such a TGSD is obtained by testing the relative weighting averages from 100% Field TGSD to 100% Radar TGSD. The best-fit is reached when the field measurements are best reproduced following a goodness-of-fit procedure (Sect. 3.3).

p. 5, line 36. "X(phi_5) is the fraction obtained for phi=5". How do you obtain this fraction? By estimating the total mass of the cloud and dividing it by the total mass of the deposit+cloud? Also, there could be a little more explanation about how PM_{20} is estimated from the integrated TGSD. If PM_{20} is at the tail of the size distribution derived from radar, it seems that the mass of PM_{20} would be highly dependent on the size distribution assumed (i.e. gamma) from the radar retrievals. TGSD's tend to be polymodal, a fact that is not considered here.

The paragraph (p.5 – lines 21-31) was reworked to gain in clarity about the empirical modification of the Integrated TGSD. We based the modification on the power-law decay, starting from $\Phi = 6$ (i.e. PM_{20}). In other words, the fractions for $-5 \leq \Phi \leq 5$ are determined by applying the relative weighting factors to the Field and Radar TGSDs, without modifying the individual TGSDs. The paragraph related to the weighting average inversion is mentioned in p.5 – lines 14-20. As described in Costa et al. (2016a), the polymodality on TGSD tends to be a common feature for most eruptions. The issue associated with the distribution used for radar

retrieval (Gamma distribution) has been described (p.5 – lines 7-13) and a better characterization of such distribution is the subject of ongoing research. In particular, as we explained in p.5 – lines 1-7, the Gamma distribution is assumed for the variables D and ND, where D(mm) is the particle diameter and N ($mm^{-1}.m^{-3}$) is the number of particles per unit of volume and particle size interval. Then, this distribution is converted in Φ, wt %. In addition, since a single Gamma distribution is not able to adequately describe large size spectra, a Gamma distribution, with different parameters, is assumed in each particle size range of fine ash, coarse ash, small lapilli, and large lapilli, so the final total distribution is a combination of several Gamma distributions. However, such an empirical derived distribution can be probably approximated using distributions different than the Gamma distribution, such as a lognormal or a Weibull distribution. The latter point will be investigated in future studies.

p. 6, line 12: "α and β are obtained empirically through the solution of an inverse problem (Poret et al., 2017)". A little more detail would be helpful. You took cases where both the plume height and eruption rate were known, and then adjusted α and β until the modeled height matched the observed one?

Throughout the simulations, we hold the column height (hence MER). The sentence was modified (p.6 – lines 2-6) to better explain how the air entrainment coefficients were used. More details on the calibration were given in the following section (e.g. p.7 – lines 12-16) about the inversion modelling strategy. α and β are inverted on the basis of the theoretical erupted mass estimated from the field samples (p.7 – lines 23-26). We used α and β ranges to make the index K converging towards 1 giving the optimal erupted mass.

p. 6, lines 24-42. The English in this paragraph really needs some work. And why are you spending so much time comparing winds over the volcano with those in Tirana?

The paragraph was reworked to edit the read (p.6 – lines 20-39). We used few lines to compare the wind conditions over the two different locations to 1) justify the benefit from such meteorological conditions during the eruption (i.e. wind speed and direction), and 2) the alternative use of the 2 meteorological databases.

Section 3.3 (p. 6, lines 10+). I think it would be valuable to show a table listing variables that were varied in your optimizations.

Thank you for pointed out the lack of visibility. We added a table to list the input parameters (now Table 2). We also edited Section 3.3 to read (p.7 – line 5).

p. 7, line 15. To quantify the goodness of fit, what observations were you comparing with model results? Cloud load? Deposit mass load? Was each observation, e.g. deposit mass load at each sample location, equally weighted with every other observation? Also, there is not enough explanation of K and k to know what they signify. It would be worthwhile to show the equations used to calculate K and k.

The comparison description was confusing. We mentioned the comparison of the tephra loadings at the sampled sites between the numerical outputs and the field measurements (p.7 – lines 10-11). Also, we clarified the goodness-of-fit procedure in p.7 – lines 17-27, and added the equations defining the indexes K and k.

p. 7, line 25. It's not exactly clear to me what simulations you are doing that attempt to reproduce "sampled tephra loadings". Are you doing plume simulations, feeding the airborne tephra into FALL3D to simulate the deposit, then comparing the simulated deposit mass load with measured values? What were the setup parameters for the FALL3D runs? What was the model domain, model resolution etc.?

We computed the tephra loading at the sampled sites, which are compared with the field measurements (p.7 – lines 10-11). We added a table listing the input parameters (now Table 2) and an Appendix indicating the complementary parameterization used within FALL3D.

p. 9, lines 8-9. What FPlume results were you comparing with observations during your simulations that constrained values of alpha and beta? The constrained ranges, alpha=0.06-0.15, beta-0.21-1.00, are so wide that I think the constraints aren't really meaningful.

To constrain the parameters α and β, we compared the tephra loading at the sampled sites. During the inversion of the Integrated TGSD, we tested the relative weighting averages for the Field and Radar TGSDs between 100% Field TGSD and 100% Radar TGSD. For such interval, we obtained α and β ranging from 0.06 – 0.15 and 0.21 – 1.00, respectively. To retrieve the best weighting average combination for the Integrated TGSD, we compared the optimal simulations in terms of theoretical TEM for all the combinations (now Table 3). For this reason, we obtained various α and β values also reported in Table 3. As a consequence of running simulations for each weighting average combination, and different α and β values, the resulting TEM also varied (Table 3). Although the different Integrated TGSDs tested contain variable amount of coarse and fine ash, the results yield range for α and β consistent with the literature (p.9 – lines 5-7).

p. 9, lines 25-30. There are several reasons why the model result could be inaccurate in the proximal region. One of them has to do with details of plume dynamics, and fallout of large clasts from the side of the rising column. How is FPlume integrated into FALL3D? Does it consider fallout from the side of the column? How does it transfer mass from the column to FALL3D? How is fine ash distributed with height? Is this determined within FPlume, and then transferred to FALL3D for lateral transport?

Among the different input parameters FPlume uses TGSD to solve mass conservation equation for each class and distribute it along the column. Then the mass related to the different particle classes at each different level is transported laterally using FALL3D. This was added in the revised version (p.5 – 33-41).

p. 10, line 8. You note here that the assumptions involved in the radar analysis add uncertainty. It would help to be specific about which assumptions are important, and how they would affect uncertainty.

X-Radar retrievals suffer from uncertainty essentially due to three main factors: radar forward model parameterization, geometry of view and instrument calibration. Although all of them are important, a complete sensitivity study on the error sources associated with X-Radar retrievals is not yet available for the community and is beyond the scope of this work. However, instrument calibration has been checked and corrections applied before processing data for the final estimation. The limitations of the geometry of view must be accepted for obvious reasons. An important role is played by the radar forward model parameterizations, which are used to reproduce synthetic signature of radar observations, and then considered to set up the retrieval

algorithm. In this respect, among others assumptions (particle shape, density, and orientation) we assumed a Gamma shaped PSD and Rayleigh particle's scattering regime to retrieve PSD parameters. Our feeling is that radar forward model assumptions mainly drive the final radar retrieval. We corrected the sentence in p.10 – lines 4-7.

Table 2: What are RMSE_1, RMSE_2, and RMSE_3? RMSE values for each of the three eruption schemes illustrated in Fig. 7? Also, I'm a bit confused about why the total erupted mass (TEM) is changing in each row of the table. Are you adjusting it until the RMSE is minimized? Are you adjusting any other parameters? Are you somehow calculating the total mass in the air from radar measurements and using that as the model input? This reinforces my view that there is a lot that needs to be explained regarding the radar data.

The different RMSEs are introduced in p.7 – lines 18-19. They refer to different error distributions as described in Folch et al. (2010). The table (now Table 3) was not well introduced, which is corrected in p.8 – line 20 (Section 4.1). We also mentioned that each combination in the table refers to the input parameter values (e.g. α and β) used to obtain the best theoretical TEM ($K \approx 1$), explaining the report in Table 3 of TEM for each weighting combination. Then, in p.9 – lines 34-39, we discussed the resulting output TEMs with the values from the literature (Andronico et al., 2015; Corradini et al., 2016).

Figure 5: Isn't the radar TGSD supposed to have a gamma distribution? It doesn't look like one. (or does the gamma distribution only apply to each volume in the radar?).

As mentioned above, the Gamma distribution has a Gamma shape in the D, ND domain, where D (mm) is the particle's diameter and N ($mm^{-1}.m^{-3}$) is the number particles per unit of volume and particle's size interval. This is why you probably do not recognize a Gamma distribution in Fig. 5, which is displayed in Φ (wt%). In addition, since a single Gamma distribution is not able to adequately describe a large size-spectra, a Gamma distribution (with other parameters) is assumed for each particle size range of fine ash, coarse ash, and lapilli. It follows that the final total distribution is a combination of several Gamma distributions.

Animation A1: How were the SEVIRI data processed to give ash mass load? Who did the processing? Why does the animation look like a model output? Should it show pixels of ash? Why is there a brown airplane off the coast of Albania?

Thank you for pointed out the confusion. We tried to display the SEVIRI retrieval time-series over the DEM to be consistent with the other animations. We corrected the animation providing the SEVIRI retrievals.

References

- Bonadonna, C., R. Genco, M. Gouhier, M. Pistolesi, R. Cioni, F. Alfano, A. Hoskulds- son, and M. Ripepe (2011), Tephra sedimentation during the 2010 Eyjafjallajökull erup- tion (Iceland) from deposit, radar, and satellite observations, J Geophys Res, 116,doi 10.1029/2011jb008462.

- Dacre, H. F., A. L. M. Grant, R. J. Hogan, S. E. Belcher, D. J. Thomson, B. Devenish, F. Marenco, J. Haywood, A. Ansmann, and I. Mattis (2011), The structure and magnitude of the ash plume during the initial phase of the Eyjafjallajökull eruption, evaluated us- ing lidar observations and NAME simulations, Journal of Geophysical Research, 116, D00U03,doi 10.1029/2011JD015608.

- Devenish, B., P. N. Francis, B. T. Johnson, R. S. J. Sparks, and D. J. Thom- son (2012), Sensitivity analysis of dispersion modeling of volcanic ash from Ey- jafjallajökull in May 2010, Journal of Geophysical Research, 117(D00U21),doi doi:10.1029/2011JD016782.

- Wen, S., and W. I. Rose (1994), Retrieval of sizes and total masses of particles in volcanic clouds using AVHRR bands 4 and 5, Journal of Geophysical Research, 99(D3), 5421-5431.

Comments from an anonymous referee (Referee 2)

Overview

This manuscript (hereafter referred to as MS) presents a method to estimate the Total Grain Size Distribution (TGSD) of volcanic ash by combining field (ash deposits) and remote sensing data (radar, and satellites). The method is applied to the paroxysmal eruption of Etna volcano, Italy on 23rd November 2013. The resulting TGSD is then used as input for a tephra dispersal model to reproduce the tephra loading and the far-field airborne ash mass. The results highlight the necessity of integrating the field and remote-sensing data (from different instrument) to achieve a better estimate of the initial TGSD, which is a key input parameter for modeling the ash dispersion and hazards.

The study is novel and within the scopes of ACP. Indeed, the integrated approach introduced in the MS can lay the ground for developing new methods or tools to assess the full spectrum TGSD, which is very important to improve the ash dispersion modeling and volcanic hazard assessment. Although the methods and assumptions seem sound and valid, they are not clearly outlined. For example, the methodology is vague in some places (please see the general comments below). So, I recommend the MS for publication after addressing the following points.

General Comments:

1. In the methodology section the text is vague and hard to follow (especially P5L20-30, P6L26-42, whole section 3.3). It could be substantially improved. Moreover, there are several tuning parameters introduced in each section and used for specific purposes. Adding one table to show these parameters, ranges and purposes would be helpful.

Thank you for having pointed out the issues. We corrected the manuscript to help the reader to follow the flow being more concise and clear, especially the methodology section (p.4 – line 28). We also added a table (Table 2) to show the input parameters used within the numerical models.

2. The authors refer to very fine ash as PM_{20} based on Rose and Durant (2009), which is a mistake. Rose and Durant (2009) define PM_{30} as the very fine ash and not PM_{20}. Authors should either justify the changes in the size range (reduced range to PM_{20}) or redo the calculations using the correct value of PM_{30}.

The introduction of the very fine ash was unclear. Although Rose and Durant (2009) define the very fine ash as PM_{30}, here we refer to the PM_{20} for consistency with the satellite data. Considering the atmospheric residence time, the range reported in Rose and Durant (2009) is still valid for PM_{20}, being included within PM_{30}. However, we corrected and referenced the use of the terms referring explicitly to PM_{20} in p.1 – lines 17-19.

3. There are references to unpublished (submitted) papers. I recommend removing these references.

Done.

4. In several locations (e.g. P4L23, P10L27), it is written that ice is released/emitted/erupted. Volcanoes never emit ice. They emit water vapor that is transformed into liquid water and ice due to microphysical processes. This could be seen also in Fig. 4 where ice formation starts later than SO_2 and ash emission. Taking this into account, how would the interpretations change?

Thank you for having raised the confusion. We corrected the sentences in p.4 – lines 4-8 and p.10 – line 19. Obviously, we meant that ice was produced by the conversion of the water vapour that ascent up to the top of the volcanic column. The interpretations that the upper water (ice) rich part moved in a different direction of the lower part remain unchanged.

5. The 1D plume model FPlume is able to reproduce the ash to ice ratio during the plume evolution. It would be interesting to see how the FPlume modeling results compare with the values shown in Fig. 4 (ice/ash ratio could be calculated from this data). This is very important for model evaluation. Indeed, the authors take a primary input (TGSD) and then try to reproduce the very last outputs: deposition and airborne mass. This means they omit all the important factors and uncertainties that affect the plume rise and transport between emission and deposition (like the ash/ice ratio mentioned above or vertical distribution of the plume). These uncertainties and simplifications should be clearly explained and justified.

The FPlume model is used to describe the source in terms of tephra particle released per unit of time at the scale of FALL3D grid, that is of a few kms. The focus is not to describe the microphysics of the column or the feature of the plume in the near field. The uncertainties related to these processes are dealt as uncertainties of the source term. A systematic parametric study about typical uncertainties in FPlume is presented in Macedonio et al., (2016). This was mentioned in the revised text (p.6 – line 9). This study aims at highlighting that a synergic use of different data permits reproducing simultaneously ground and airborne observations. Although uncertainties affecting the plume and tephra transport between emission and deposition exist, on the scale of our simulations, local plume dynamics and plume microphysics are not pivotal and our approach aims at constraining the plume height and MER by reproducing available field and airborne measurements. Factors that can affect plume at local scale (lower than FALL3D resolution considered in this study) should be investigated using more sophisticated models (e.g. Cerminara et al., 2016), not using simplified BPT models.

Specific comments

P1L02: do you mean “explosive volcanic eruptions”?

Yes, we corrected in p.1 – line 15

P2L05: replace automatic with automated.

Done (p.2 – line 5).

P2L08: By Making ...

Done (p.2 – line 8).

P2L41-P3L2: This belongs either to the abstract or conclusions.

Done. The sentences were modified and moved to the abstract (p.1 – lines 24-30).

P3L10: 17th episode in the history or in one specific duration?

The paroxysm is the 17th of the specific duration of 2013, as mentioned in p.3 line 2.

P3L16: "heavier" or denser?

Thank you for pointed out the confusing terms. The brownish cloud is denser than the water vapour cloud. We corrected the sentence in p.3 – line 8.

P3L17: Volcanoes do not emit any water/gas droplets. Water droplets and aerosols are indeed formed in the atmosphere.

The sentence was corrected in p.3 – line 9.

P6: What are the input parameters of FPlume (exit velocity, vent diameter etc)? Please explain.

The model FPlume, the assumptions, input parameters, and limitations are extensively described in other papers cited in the main text (Folch et al., 2016; Macedonio et al., 2016). As input, it needs the TGSD, the eruptive column height (or MER), initial ejection velocity, exit magma temperature, and water fraction at the vent. These points were better described and the section related to the use of FPlume improved (from p.5 – line 33).

P6L8: 2.5 wt% of what? Water?

The sentence was corrected (p.6 – line 1).

P6L13: This is not clear. Do you mean less that 2 wt% of the fine ash is removed by aggregation?

Yes, 2 wt% of the fines are removed by aggregation as described in Poret et al. (Under review). The sentence was modified to gain in clarity (p.6 – lines 6-8).

P8L23: what is the difference between RMSE1, 2 and 3? Please explain.

Thank you for having mentioned the issue. The difference between the RMSEs is related to the error distribution used within the calculation. The full description of the different RMSEs is available in Folch et al. (2010), although we modified the sentence in p.7 – lines 18-19.

Fig. 3: The quality is so low that the ash and ice plumes are very hard to recognize. Please use a higher resolution if available.

Thank you for having pointed out the lack of visibility. We modified the figure and hope the reader can appreciate the figure showing the dispersion of the ash and ice clouds.

Fig. 5: please clarify the difference between Whole TGSD and the integrated TGSD in the text.

The TGSD section (Sect. 3.1 in p.4 – line 34) was modified to improve the clarity about the difference between the TGSDs. In particular, the Integrated TGSD emerges from the weighting average combination between the field-derived TGSD and the X-Radar-derived TGSD. The Integrated TGSD is inverted by best-reproducing the tephra loading at the sampled sites (p.5 – lines 14-20). Then, the Whole TGSD is the empirical modification of the Integrated TGSD by adding very fine ash into the tail of the distribution to best reproduce the airborne ash mass retrieved from satellite (p.5 – lines 21-31).

Reconstructing volcanic plume evolution integrating satellite, and ground-based data: Application to the 23rd November 2013 Etna eruption

Matthieu Poret[1, 2], Stefano Corradini[3], Luca Merucci[3], Antonio Costa[1], Daniele Andronico[4], Mario Montopoli[5], Gianfranco Vulpiani[6], and Valentin Freret-Lorgeril[7]

[1]Istituto Nazionale di Geofisica e Vulcanologia, Bologna, Italy
[2]University of Bologna, Geophysics department, Bologna, Italy
[3]Istituto Nazionale di Geofisica e Vulcanologia, CNT, Roma, Italy
[4]Istituto Nazionale di Geofisica e Vulcanologia, OsservatorioEtneo, Catania, Italy
[5]Institute of Atmospheric Sciences and Climate, National Research Council of Italy, Roma, Italy
[6]Department of Civil Protection, Presidency of the Councils of Ministers, Roma, Italy
[7] Université Clermont Auvergne, CNRS, IRD, OPGC, Laboratoire Magmas et Volcans, F-63000 Clermont-Ferrand, France

Correspondence to: Matthieu Poret (matthieu.poret@gmail.com)

Abstract. Recent explosive volcanic eruptions recorded ~~from different volcanoes~~ worldwide (e.g. Hekla in 2000, Eyjafjallajökull in 2010, Cordón-Caulle in 2011) demonstrated the necessity of a better assessment of the Eruption Source Parameters (ESP; e.g. column height, mass eruption rate, eruption duration, and Total Grain-Size Distribution – TGSD) to reduce the uncertainties associated with the far-travelling airborne ash mass. ~~To do so, v~~Volcanological studies started to integrate observations to use more realistic numerical inputs, crucial for taking robust volcanic risk mitigation actions. On 23rd November 2013, Etna volcano (Italy) erupted producing a 10-km height plume, from which two volcanic clouds were observed at different altitudes from satellite (SEVIRI, MODIS). One was ~~described~~ retrieved as mainly composed by very fine ash (i.e. PM_{20}), whereas the second one as made of ice/SO_2 droplets (i.e. not measurable in terms of ash mass). Atypical north-easterly wind direction transported the tephra from Etna towards the Calabria and Puglia regions (southern Italy), permitting tephra sampling in proximal (i.e. ~5-25 km from source), and medial areas (i.e. Calabria region, ~160km). A primary TGSD was derived from ~~Based on~~ the field ~~data~~ measurement analysis, ~~we estimated the TGSD~~ but the paucity of data (especially related to the fine ash fraction) prevented it from being entirely representative of the initial magma fragmentation. For better constraining the TGSD assessment~~To better estimate the TGSD covering the entire grain-size spectrum, we integrated the available field data with X-band weather radar and satellite retrievals. To assess the TGSD associated with the 23rd November 2013 paroxysm (together with the other ESPs)~~, we ~~first~~also estimated the ~~grain-size~~ distributions ~~derived~~ from ~~i) field and ii)~~the X-band weather radar ~~X-Radar~~ data~~, respectively~~. ~~Then, w~~We integrated the~~m~~ field and radar-derived TGSDs by inverting the relative weighting averages~~the two distributions~~ to best-fit the ~~measured~~ tephra loading measurements. The resulting TGSD is used as input for the FALL3D tephra dispersal model to reconstruct the whole tephra loading. Furthermore, we empirically modified the ~~resulting~~integrated TGSD by enriching the PM_{20} classes until the numerical results were able to reproduce the airborne ash mass retrieved from satellite data. ~~The resulting TGSD is used as input for the FALL3D tephra dispersal numerical model to reconstruct the tephra loading and the far-travelling airborne ash mass.~~ The ~~optimal~~ resulting TGSD is ~~selected~~ inverted ~~by solving an inverse problem through a~~ best-fitting ~~with~~ the field, ground-based, and satellite-based measurements. The results ~~suggest~~ ~~suggest~~indicate a total erupted mass of 1.2 × 10^9 kg, ~~which is very~~being similar to the field-derived value of 1.3 × 10^9 kg, ~~also~~and an initial ~~, and a TGSD with a~~ PM_{20} fraction between 3.6 and 9.0 wt%~~, to use within~~ constituting ~~the~~ tail of the TGSD.~~.~~

Keywords: TGSD; FALL3D; SEVIRI; PM_{20}; tephra dispersal modelling; ~~Eruption~~ eruption ~~Source~~ source ~~Parameters~~parameters

1 Introduction

Volcanic explosive eruptions pose hazards related to the release of large quantity of material into the atmosphere. ~~During such events, t~~The observation of the eruption features, such as the eruptive column, the tephra ~~fallout deposit~~loading, ~~and~~ or the far-travelling volcanic plume aims at characterizing the Eruption Source Parameters (ESP). Hazard assessment related to tephra dispersal, and its implications for aviation safety and public health, is one of the major motivations for developing robust automated~~ie~~ tools to forecast tephra loading and airborne ash dispersal ~~and tephra loading~~ (e.g. ~~Macedonio et al., 2005;~~ Costa et al., 2006; Barsotti et al., 2008; Folch et al., 2008; 2009). ~~In order t~~To mitigate the risk to aviation traffic, nine VAACs (Volcanic Ash Advisory Centers) were created worldwide for volcanic cloud monitoring purposes. By ~~Making~~ making use of operational volcanic ash transport and dispersion models, VAACs aim at alerting for the presence of volcanic ash in the atmosphere. ~~Ideally, as input (Folch, 2012), beside~~ Beside other ESPs (e.g. eruption start and duration, ~~and~~ column height, and ~~or~~ Mass Eruption Rate – MER), ~~such~~ such models require the Total Grain-Size Distribution (TGSD) as input (e.g. Folch, 2012), ~~which already has demonstrated to represent~~being one of the most critical ESPs, significantly affecting tephra dispersal model outputs (e.g. Scollo et al., 2008; Beckett et al., 2015). Typically, the TGSD is derived from the field sample analysis through the Voronoi tessellation method (Bonadonna and Houghton, 2005). However, collecting field data on tephra deposit highly depends on the atmospheric conditions, land/sea deposition, site accessibility, etc. As a consequence, for inadequate ~~when the~~ sample dataset ~~is not adequate~~ in terms of sampling distance from the source (Andronico et al., 2014; Costa et al., 2016a), spatial distribution and density of samples (Bonadonna et al., 2015, Spanu et al., 2016), the field-derived TGSD is uncertain and cannot be assumed as representative of the whole tephra loading and dispersal. Additionally, the atmospheric residence time of the very fine ash (i.e. hereinafter in this work PM_{20}~~-~~), ranging from hours to weeks~~;~~ (Rose and Durant, 2009) prevents from any rapid deposition implying their substantial under-estimation within the TGSD (Bonadonna et al., 2011~~; Poret et al., Submitted~~). This raises the necessity ~~of~~ for integrating field data with measurements from other sensors (e.g. ground-based radar and satellite) capable to retrieve the missing information in terms of airborne ash. Moreover, ~~Recent~~ the recent eruptions (e.g. Hekla in February 2000, Eyjafjallajökull in April 2010, Cordón-Caulle in June 2011) have shown the impact of the very fine ash on air traffic (e.g. Guffanti et al., 2010; Folch et al., 2012; Sulpizio et al., 2012), but also on public health (e.g. respiratory diseases; Andronico and Del Carlo 2016~~; Horwell et al. 2017~~; Tomašek et al. 2016; Horwell et al. 2017).

The non-existence of a single instrument capable to cover entirely the grain-size spectrum motivated~~brings~~ this study in proposing a method based on the synergic use of field, ground-based, and satellite data for better constraining the TGSD, and therefore the numerical simulations (here FALL3D; Costa et al., 2006; Folch et al., 2009)~~From a computational point of view, the reconstruction of the tephra loading and far-travelling airborne ash dispersal is made by considering a set of ESPs, such as the eruption start and duration, the column height or the Mass Eruption Rate (MER) and the TGSD. This study aims at better constraining the TGSD estimation by integrating field, ground-based and satellite-based measurements.~~ to reconstruct the tephra loading and the far-travelling airborne ash dispersal. ~~In fact, the non-existence of a single method capable to cover entirely the grain-size spectrum implies such a TGSD should be estimated through an integrated approach. Although~~Actually, excluding a few studies (Bonadonna et al., 2011; Folch et al., 2012~~; Poret et al., Submitted~~), ~~tephra dispersal~~ simulations are commonly run by using the field-based TGSD or adopting subjective parameterizations (e.g. assuming a constant mass fraction for fine ash).~~;~~ ~~here~~ Here, we expanded the reconstruction of the tail of the field-derived TGSD by using radar ~~retrievals~~ and satellite retrievals~~measurements~~.

~~Our~~ We applied this methodology ~~is applied to~~to the 23rd November 2013 Etna paroxysm, which occurred ~~on the early morning through~~ from the New South-East Crater (hereinafter NSEC), being the most active crater in the last 20 years (Behncke et al., 2014; De Beni et al., 2015). Atypical winds dispersed the plume north-easterly driving the tephra towards the Calabria and Puglia regions (~400 km from the source), where ash fallout was reported (Bonaccorso et al., 2014; Andronico et al., 2015; Montopoli, 2016). ~~After~~ Few hours after the eruption, tephra was ~~samples~~ sampled ~~were collected~~ along the plume axis from ~~the volcanic slopes~~Etna (i.e. 5-25 km from NSEC) to Calabria (i.e. ~160 km; Fig. 1 and Table 1). Meanwhile, the eruption benefited from being observed through ground-based (i.e. X-band weather radar – X-Radar and L-band Doppler radar – VOLDORAD 2B) and satellite-based (i.e. infrared satellite radiometer) remote sensing instruments. Although they operate in different parts of the electromagnetic spectrum, their integration aims at providing a more complete view of the eruption, especially of the plume dynamic.

In Section 2,~~This work aims at producing a constrained TGSD emerging from the integrated approach to reconstruct the tephra loading and the airborne ash dispersal by using the FALL3D tephra dispersal model (Costa et al., 2006; Folch et al., 2009). To assess the TGSD associated with the 23rd November 2013 paroxysm (together with the other ESPs) we first estimated the grain-size distributions derived from i) field and ii) X-Radar data, respectively. Then, we integrated them by weighting the two distributions to best-fit the measured tephra loadings. Furthermore, we empirically modified the resulting TGSD by enriching the PM_{20} classes until the numerical results reproduce the airborne ash mass retrieved from satellite data. In the scope of assessing the complete initial TGSD, the individual distributions (i.e. field- and radar-derived TGSDs) cannot cover entirely the grain size spectrum, motivating its achievement by the synergic use of the field, ground based, and satellite retrievals.~~

~~T~~the paper ~~is organized as follows:~~presents ~~in Section 2 describes~~ the 23rd November 2013 Etna eruption, the field and remote sensing data ~~and the field measurements~~. Section 3 reports the TGSD estimation, the model~~l~~ling approach and methodology used to reproduce the eruption features. Section 4 is devoted to the results together with their discussions. Section 5 presents the main concluding remarks.

2 The 23rd November 2013 lava fountain

In 2013, the 17th lava fountain episode took place on 23rd November from the NSEC (De Beni et al., 2015). Mild Strombolian explosions initiated on 22nd November afternoon and increased after 07:00 of the following day (all times are in UTC). The transition between Strombolian and lava fountaining activity (i.e. between resumption and paroxysmal phase~~s~~; Alparone et al., 2003) started at 09:30, producing intense lava fountains which increased rapidly in height and intensity. During the 50 min of duration of the ~~(~~paroxysmal phase~~)~~, a sustained 10-km height eruptive column was observed (Bonaccorso et al., 2014; Andronico et al., 2015). ~~Nonetheless~~Moreover, a peculiar feature was recorded ~~(e.g. surveillance cameras~~ from INGV–OE~~,)~~ ~~for this paroxysm by~~ showing a ~~whitish~~ greyish volcanic plume that rose above a denser brownish one ~~(heavier)~~, from which tephra fallout was visible (Fig. 2). Such observation is attributed to the release of a large amount of water vapour/gas ~~droplets~~ rising higher than tephra (Corradini et al., 2016). This is relevant for characterizing the far-travelling airborne ash, which becomes more complex with the presence of two distinct volcanic clouds. ~~Additionally~~In this case, ~~the presence of~~ volcanic ash in the far-field region~~s~~ was testified by a A319 pilot ~~who flew~~flying over the Albanian coasts at 13:50 ~~at~~ and 10.3 km above ~~sea~~ level (a.s.l.), i.e. ~~(~~FL 339~~)~~, ~~who~~ report~~ed~~ing ash between 10.9-11.5 km a.s.l., i.e. FL 360-380 (Crompton and Husson, 2015). ~~The following sub-sections describe the observational data used for this study.~~

2.1 Field data

Samples were collected and tephra loading per unit area measured at 7 locations (Fig. 1 and Table 1). They were oven-dried at 110 °C for 12 hours and ~~analysed~~analysed in the ~~Sedimentology~~ sedimentology ~~Laboratory~~ laboratory at INGV-OE, in

Catania (Italy). The individual Grain-Size Distributions (GSD; available as supplementary material in Fig. S1) were ~~analysed~~measured optically at 1 Φ-interval through the CAMSIZER® (Retsch Technology), covering the range from -5 to 5 Φ (where $d = 2^{-\Phi}$, with the diameter d in mm). Although field measurements are commonly used for determining the Total Erupted Mass (TEM) by integrating the isomass lines (Bonadonna and Costa, 2012; 2013), the paucity of samples ~~together~~ with their wide dispersion (Fig. 1) limits the reliability of the estimation based on field observations only. However, on the basis of the field data analysis, Andronico et al. (2015) estimated a TEM of $1.3 \pm 1.1 \times 10^9$ kg making use of the Weibull distribution method (Bonadonna and Costa, 2012; 2013). Then, combining the field-derived TEM with the paroxysmal duration (~50 min), they calculated an average MER of $4.5 \pm 3.6 \times 10^5$ kg/s ~~(Andronico et al., 2015)~~. Furthermore, considering the climax phase only (i.e. from 09:55 to 10:14), the MER ~~goes~~ reached~~up to~~ 10^6 kg/s ejecting more than 80 wt% of the erupted mass (Donnadieu et al., 2017). It is worth noting that such MER estimations represent average (or peak) value for the entire duration of the paroxysmal phase without ~~and do not~~ considering its time evolution (i.e. the variation of eruption intensity). Indeed, ~~in our case~~ the ~~eruption intensity increased and the~~ time-series MER can be assessed from the relationships between MER and the column height (e.g. Mastin et al., 2009; Degruyter et al., 2012; Woodhouse et al., 2013; Folch et al., 2016) and from velocity variations at the vent recorded by ~~the Doppler radar~~ VOLDORAD 2B. ~~Hence, to account for the eruptive intensity variation, the calculation would benefit from integration of plume models with measurements of remote sensing systems, which is proposed in this study.~~

2.2 Satellite and ground~~-~~based remote sensing data

The simultaneous record of the eruption ~~was simultaneously observed~~ from both satellites and ground-based instruments permits retrieving. ~~O~~ On the first hand, ~~the satellite measurements of~~the plume spreading and airborne ash mass dispersal (see Animation A1 in the supplementary material), ~~were~~ collected ~~making use of~~by the Spinning Enhanced Visible and Infrared Imager (SEVIRI) on board the geostationary Meteosat Second Generation (MSG) satellite. The Moderate Resolution Imaging Spectro-radiometer (MODIS) aboard the NASA-Aqua polar-orbit satellite was also used to describe the eruption features (Corradini et al., 2016).

On the second hand, concerning ground-based instruments, the X-Radar (Montopoli 2016, Vulpiani et al., 2016) and the visible/thermal cameras (Corradini et al., 2016) ~~were used to~~ provided time-series data of the plume height and the erupted mass.

T~~T~~he available~~se observations~~data mentioned above were integrated through a multi-disciplinary approach in Corradini et al. (2016) to improve the volcanic cloud retrievals, the source characterization and to generate new products ~~based on the multi-disciplinary approach described in Corradini et al. (2016)~~. In particular, the satellite ~~measurements~~ observations ~~associated with this eruption~~ (Fig. 3) ~~observed~~ showed~~n~~ the~~the~~ formation of the two distinct volcanic clouds described in Sect. 2. Although both ~~moving at their own altitudes~~spread ~~towards~~ north-eastwards. ~~Among these two clouds, o~~ one ~~appears to~~ reached ~6 km a.s.l. ~~(above sea level),~~ being mainly ~~composed by~~made of ash (Ash Cloud – AC), and therefore ~~observable~~ retrieved~~from satellite~~ in terms of airborne ash mass and cloud altitude. The second cloud ~~is~~ was higher (~11 km a.s.l.) ~~and made~~ with ~~of~~ enough ice/gas droplets (Ice/gas Cloud – IC) to significantly alter~~with a dominant~~ the cloud characteristics ~~significantly different from the AC,~~ blinding the satellite from any ash mass measurement (Prata ~~et al.~~and Kerkmann, 2007). ~~As observed a~~Initially~~t the source~~, the clouds were united and split out over the Calabria region (around 11:00). ~~As~~ In a final stage, the AC reached the Puglia region, whereas the IC moved over the Ionian Sea towards Albania (around 14:00). In terms of mass, Fig. 4 shows ash was dominant from the onset of the eruption until 11:30, and then ice replaced ash. In fact, from SEVIRI retrievals, ash was likely released between 10:00 and 12:00 prior the emitted water vapour was transformed into ice (i.e. 11:00-12:45). This is also shown in Fig. 4, where ice formation starts later than SO_2 and ash emission. SO_2 was released all along the eruption (i.e. 10:00-12:30), although with a lower contribution than ash and ice.

-The data integration presented in Corradini et al. (2016) permits to reduce the uncertainties associated with the vVolcanic ~~Cloud~~ cloud tTop hHeight ~~(VCTH)~~, the ~~volcanic~~ ash/ice/SO_2 mMasses (~~M_a, M_i and M_s in~~ Fig. 4) and the Aerosol Optical Depth (AOD) retrievals. On the basis of the satellite and X-Radar data, Corradini et al. (2016) improved the mass estimation of 30 % and reported a X-Radar-derived TEM of ~3.0 × 10^9 kg with a PM_{20} fraction between 1-2 wt%, that is ~30~~0~~-60~~0~~ tons ~~in weight~~. ~~From the onset of the eruption, Fig. 4 shows that ash was dominant until 11:30, from which ice replaced ash. In fact, ash was likely released between 10:00 and 12:00 prior ice (i.e. 11:00-12:45). SO_2 was released all along the eruption (i.e. 10:00-12:30) but the retrievals inferred a lower contribution with respect to the ash and ice. In addition to the VCTH assessment,~~ tThe source characterization also ~~needs~~ can ~~to~~ be better ~~estimated~~ described by means ~~through~~ of the ESP ~~together with~~and the eruptive phases. ~~To do so,~~ tThe plume height time-series ~~is~~ was recorded from the visible cameras ~~of the~~at INGV-OE, ~~which~~ indicatinge values ~~ranging~~ from the NSEC (~3300 m a.s.l.) ~~up~~ to ~11 km a.s.l., with a rapid increase around 9:30 followed by a decay at 10:20.

~~Besides SEVIRI and X-Radar retrievals, the eruption was also observed through t~~The VOLDORAD 2B radar is~~. In particular, this~~ a pulsed Doppler radar ~~operates~~ operating ~~in the~~at 23.5-cm wavelength ~~of 23.5 cm~~ (L-band) allowing lapilli to block-sized to be ~~observed~~detected. VOLDORAD 2B ~~is~~ continuously ~~monitoring~~ monitors Etna's summit craters since 2009 (Donnadieu et al., 2015; 2016) ~~from la Montagnola Station, which is~~ at 3 km from the NSEC (La Montagnola Station)~~)~~. Inferred radar parameters (e.g. backscattered echo power) are proportional to the quantity of tephra detected through the radar beam. In addition, the along-beam radial velocities permit lava fountains from being observed at high time resolution (i.e. 0.2 s), inferring near-source detection of the ejection velocities by means of the following equation (Freret-Lorgeril et al., 2016; Donnadieu et al., 2017):

$$V_e = \frac{v_{r+}}{\sin\theta} \approx 3.89 v_{r+} \quad (1)$$

where V_e is the ejection velocities (in m/s), v_{r+} is the radial velocity (in m/s) and θ is the elevation angle of the radar beam (here $\theta = 14.9°$). Such approach is relevant for integrating the time-~~dependant~~dependent ejection velocities with the corresponding observed eruptive column heights. In particular, we used the VOLDORAD 2B data associated with the 23rd November 2013 eruption to better constrain the eruption phases characterization.

3 Methodology

~~To s~~Simulat~~e~~ing the tephra loading and airborne ash dispersal ~~related to~~of the 23rd November 2013 Etna eruption~~, we need~~ requires to ~~know~~ assess the related ESPs, and in particular the TGSD. Their use as input parameters into the FPlume model (Folch et al., 2016) aims at describing the eruption column, representing the source term ~~through the FPlume model (Folch et al., 2016), which is~~ required by the FALL3D tephra dispersal model (e.g. Costa et al., 2016b). In the following methodology, we present the ~~i)~~ TGSD reconstruction ~~used~~ and ~~within the ii)~~ model~~l~~ling approach. Then, the ~~iii)~~ simulations are analys~~z~~sed in terms of tephra loadings and airborne ash mass dispersal to best-fit the field and satellite measurements.

3.1 TGSD estimation

~~As mentioned above, although~~The ~~the paucity and spatial distribution prevent the~~ 7 field samples are not sufficient ~~from~~ for ~~representing~~ assuming ~~fully~~ the field-derived TGSD as the full spectrum ~~whole~~ TGSD (Andronico et al., 2014; Beckett et al., 2015; Bonadonna et al., 2015; Costa et al., 2016a; Spanu et al., 2016~~),~~). Although such a field-based TGSD is being biased toward coarse ash, we first estimated the TGSD (hereinafter Field TGSD; Fig. 5) ~~on the basis of~~from the individual GSDs using the Voronoi tessellation method (Bonadonna and Houghton, 2005). However, the Field TGSD needs to be ~~improve~~better characterized prior to be used within ~~numerical models~~atmospheric ash dispersal models. ~~However,~~ ~~e~~Considering ~~the partial~~ the Field TGSD representativeness ~~of the~~on the grain-size spectrum (i.e. -5 to 5 Φ; Sect. 2.1)~~Field~~

~~TGSD on the erupted material~~, ~~the~~ we used the X-Radar retrievals to constrain the mass ~~information on particle grain-size~~ relative to coarse and fine ash (~~defined in~~ i.e. -1 to 5 Φ; Corradini et al., 2016~~Rose and Durant, 2009~~) ~~are retrieved by means of the X-Radar data~~. The X-Radar-derived TGSD is inverted from the Particle-Size Distribution (PSD), given ~~In fact, the X-Radar measurements can provide the Particle-Size Distribution (PSD)~~ as ash number density distribution ~~in $m^{-3} \cdot mm^{-1}$~~ (Corradini et al., 2016). ~~However,~~ It is worth noting that we considered a spatial and temporal average of the X-Radar-based PSD for the whole event. The average takes in input each PSD estimated from each single radar resolution volume delineated by horizontal angle, vertical angle, and range distance at each available time step for the airborne ash mass seen by the radar. ~~w~~We converted the PSD into number of particles per unit of volume ~~through~~with the particle-size bins. Then, ~~B~~by means of the volume and density associated with the size bins, we calculated the mass density distribution (hereinafter Radar TGSD; Fig. 5). ~~the X-Radar-derived PSD also suffers from such partial representativeness of the tephra due to the PSD retrieval uncertainty related to i) the simplifications in the shape of the PSD, which is assumed equal to a gamma distribution model, ii) the Rayleigh particle's scattering regime used to retrieve the PSD parameters and iii) the representability of the model regressions used for parameterizing the PSD parameters as a function of radar measurements~~. However, we would like to highlight that retrieval of Radar data is done assuming a Gamma distribution for the number particles per unit of volume for each particle size interval. Then this distribution is converted to express the mass fraction as function of Φ. In particular, since a single gamma distribution is not able to adequately describe large size spectra, a ~~g~~Gamma distribution, with different parameters, is assumed in each particle size range of fine ash, coarse ash, small lapilli, and large lapilli, so the final total distribution is a combination of several gamma distributions. However, such an empirical derived distribution can be approximated using other distributions, such as a lognormal or a Weibull distribution. The latter point will be investigated in future studies.

~~Then, to retrieve the TGSD from the X-Radar distribution, we converted the PSD into number of particles per unit of volume through the particle-size bins. By means of the volume and density associated with the size bins, we calculated the mass density distribution (hereinafter Radar TGSD; Fig. 5).~~ It is worth noting that the~~se two~~ Field and Radar TGSDs ~~reflect the grain-size~~are distributions observed through their own grain-size window, which~~the field sampling (i.e. -5 to 5 Φ) or the X-Radar instrument (i.e. -1 to 5 Φ; Corradini et al., 2016), respectively.~~ ~~This observation~~ explains the substantial difference ~~of the two TGSDs~~in shape (Fig. 5). It follows that assessing accurately the ~~initial~~ TGSD covering both windows, can be done by integrating the Field and Radar TGSDs only. Although, in principle, their integration is possible, the ~~different operative~~ grain-size windows discrepancy prevents ~~them~~ from ~~being~~ merg~~ed~~ing the Field and Radar TGSDs without knowing the~~ir~~ relative weighting averages. ~~This observation explains the substantial difference of the two TGSDs (Fig. 5). Indeed, their integration require the relative weights of the two TGSDs, which is~~We determined empirically the weight combination by ~~considering~~ ~~integrated~~ integrating the distributions at regular intervals (i.e. ~~ranging~~ from full Field TGSD to full Radar TGSD). The resulting distribution (i.e. -5 to 5 Φ; hereinafter Integrated TGSD; Fig. 5) is obtained best-fitting ~~o do so, we investigated the weights at regular intervals until we best fit~~ the ~~field~~ tephra loading at the sampled site~~measurement~~s ~~maintaining the shape of the Radar TGSD on the proper grain-size interval (hereinafter Integrated TGSD; Fig. 5)~~.

However, due to the instrument/method grain-size limit, none of the three TGSDs ~~estimations~~ (Field, Radar, or Integrated TGSD; Fig. 5) contains enough ~~a~~ PM_{20} ~~fraction enough~~ to reproduce the far-travelling airborne ash mass ~~detected~~ retrieved by satellite. ~~As in Poret et al. (Submitted)~~W~~, w~~e assessed the tail of the Integrated TGSD (i.e. $\Phi \geq 6$) by modifying empirically the PM_{20} fraction, ~~and~~ adding mass into the corresponding classes ~~(i.e. $\Phi \geq 6$)~~. We calculated the fractions based on an empirical power-law dependence of the classes with Φ through the following parameterization:

$$X(\Phi_i) = X(\Phi_5) \times \gamma^{(\Phi_i - \Phi_5)} \quad (2)$$

where $X(\Phi_i)$ is the fraction (in wt%) allocated to the i^{th} bin, $X(\Phi_5)$ is the fraction obtained for $\Phi = 5$ and γ is the empirical factor ($\gamma < 1$). The explored γ values span from 0.1-0.7, giving respectively PM_{20} fractions ~~range~~ between ~0.6-10.7 wt% of

the TEM. ~~and t~~The ~~optimal~~ best fraction to use within the TGSD (hereinafter Whole TGSD; Fig. 5) is chosen ~~on the basis of the reproducibility of both the field and~~best-fitting the satellite ~~measurements~~retrievals.

3.2 Modelling approach

To furnish the ESPs required by the FALL3D tephra dispersal ~~As input~~model, ~~FALL3D requires an estimation of the ESPs characterising the source (e.g. Costa et al., 2016b). For this aim~~, we ~~coupled~~ used ~~FALL3D with~~ the integral plume model (~~F~~Plume (~~;~~ Folch et al., 2016)~~, which~~ describ~~es~~ing the eruptive column ~~on the~~ bas~~edis~~ ~~of~~ on the buoyant plume theory (Morton et al., 1956). ~~In particular,~~ FPlume solves a set of 1D cross-section-averaged equations ~~describing~~ for mass, momentum, and energy conservation in the eruption column, accounting for wind coupling, air moisture, particle re-entrainment, and ash aggregation effects (Folch et al., 2016). Among the source conditions, FPlume feeds into FALL3D by ~~To~~ describ~~e~~ing the mass flow rate for each particle bin and the vertical distribution within the column.~~,~~ As inputs, FPlume ~~needs~~ uses ~~inputs~~ the~~(e.g. the~~ TGSD, ~~with the~~ initial magma temperature, and water content (~~;~~ Table 2) to calculate the mass releas~~ais~~ed per unit of time within the column. Indeed, FPlume uses the TGSD to solve the mass conservation equation for each class distributing along the column. Then, the mass for each particle class at each level is transported laterally using FALL3D.

In our case, Etna's magmas have a temperature of 1300 K with ~2.5 wt% of water (Carbone et al., 2015; Spilliaert et al., 2006). FPlume ~~can~~ calculates ~~the~~ MER from the column height (or vice versa) for a given wind profile (Folch et al., 2016) by describing the air mixing within the plume through two turbulent air entrainment coefficients (i.e. radial – α and cross-flow – β; Bursik, 2001; Kaminski et al., 2005; Suzuki and Koyaguchi, 2015; Folch et al., 2016; Costa et al., 2016b~~; Macedonio et al, 2016~~). ~~The uncertainties related to the microphysics of the column or the feature of the plume in the near-field are dealt as uncertainties of the source term, which are described in Macedonio et al. (2016). In our study~~Here, α and β are obtained empirically through the solution of an inverse problem ~~(Poret et al., 2017)~~best-fitting the erupted mass derived from the field measurements (Poret et al., 2017). Ash aggregation ~~is expected~~can be considered ~~to be~~ negligible during Etna eruptions with less than 2 wt% ~~with respect to~~of the fine ~~particles~~ ash removed by aggregation~~(Poret et al., Submitted)~~. For this reason, we did not consider such process in this study. The effect of the typical uncertainties associated ~~to~~with the input parameters of FPlume on the source term characterization are described in Macedonio et al. (2016).

FALL3D is used for simulating ~~Tephra~~ tephra dispersal ~~is simulated making use of FALL3D~~, ~~which~~ and is a 3D time-dependent Eulerian model based on the advection-diffusion-sedimentation equation computed over a terrain-following domain (Costa et al., 2006; Folch et al., 2009). Besides the ESPs, FALL3D needs the time-dependent meteorological fields over the computational domain for the corresponding period (i.e. from 00:00 on 23rd up to ~~24~~00:00 on ~~28th~~ 29th November 2013). The first series of simulations are run by means of a local high-resolution meteorological database (ARPAE from INGV-OE) ~~aim~~ to ~~at~~ better constraining the computed tephra loadings against the field measurements in proximal and medial areas (Fig. 1 and Table 1) ~~through a local meteorological database (ARPAE from INGV-OE)~~. Indeed, ARPAE provides a ~~high spatial (~~7 × 7~~-~~km spatial~~)~~ and 15-minutes temporal ~~(15 min)~~ resolution over the domain highlighted in Fig. 1. Then, FALL3D internally interpolates the meteorological data over a grid ~~of~~ set at 1 × 1~~—~~km resolution. The parameterizations used for the simulations with the ARPAE database are~~is~~ summarized in the Appendix. The related main atmospheric profiles (e.g. temperature, air moisture and wind speed) over the NSEC are displayed in Fig. 6~~. The use of such high-resolution meteorological field aims at better capturing the tephra loadings in the proximal and medial areas (Fig. 1 and Table 1)~~.

~~In t~~The second series of simulations~~, our goal was to~~ aims at ~~reproduce~~ reproducing the satellite retrievals, expanding the computational domain to Albania. ~~for which t~~The ARPAE ~~local domain~~data ~~(ARPAE) is~~ does not ~~adequate~~ fit cover such a ~~anymore~~domain, ~~for extending up to Albania at such spatio temporal resolution.~~implying th~~e~~for which we use ~~The~~ the meteorological fields ~~for the latter domain were obtained~~ from the European Center for Medium-range Weather Forecasts

(ECMWF, ERA-Interim-Reanalysis; hereinafter ERA-Interim). They provide 6-hour interval for 37 pressure levels data at 0.75° horizontal resolution. For computational cost reason, ~~The~~ the internal grid resolution into FALL3D is set at 5 × 5 km, which still consistent with the satellite data resolution (3 × 3 km at nadir). The parameterization used with the ERA-Interim database is summarized in the Appendix.

~~For checking t~~The consistency between the two databases is checked ~~, we~~ adding ~~added~~ the profiles retrieved over the NSEC ~~from~~ with ERA-Interim in Fig. 6. Although ~~both~~ ARPAE and ERA-Interim tend to have the same temperature and wind speed patterns, the air moisture from ERA-Interim is slightly lower than ARPAE for 3-6 km a.s.l. and higher for 7-11 km a.s.l.~~. Nonetheless, t~~These observations are not significant to produce a substantial effect on the simulations. ~~In addition to the meteorological database comparison~~Moreover ~~over the NSEC~~, Fig. 6 also shows ~~also~~ the conditions over the Albanian capital (Tirana). ~~Based on the pilot report mentioning ash,~~ With such meteorological conditions, a~~a~~irborne ~~the time necessary for the~~ tephra needs 4:30 h to be transported from Etna ~~over~~ to Albania ~~is estimated to be of 4:30 h explaining such the time shift discrepancy ion~~ (Fig. 6), being consistent~~.~~ with the pilot report mentioning ash. ~~Regardless the database, T~~~~the w~~Wind speed~~s were~~is ~~indicates~~ moderate to strong, ~~wind conditions~~ with higher velocities near the volcano ~~in contrast to~~than at Tirana city. As indicative values ~~for~~ at 9 km a.s.l., we report ~48 and ~45 m/s over the NSEC (at 09:30) for ERA-Interim and ARPAE, respectively, and ~34 m/s over Tirana city at 14:00. ~~In addition to~~Besides the velocities, the wind direction (Fig. 6) shows a strong north-easterly orientation over the NSEC, which is consistent with the tephra dispersion towards Calabria. ~~Moreover, the~~ The profiles indicate a ~~visible~~ substantial variation between mid- (5-6 km a.s.l.) and high-altitudes (> 7 km a.s.l.), which probably resulted on the different spreading orientations for the two volcanic clouds (AC and IC) at their own altitudes ~~(as described in~~ Fig. 3). Besides the profiles, the consistency for using alternatively the two meteorological databases is checked by constraining the simulations with ERA-Interim to converge the TEM towards the same value as for the Integrated TGSD and the ARPAE database. ~~Over Albania, the wind orientation shows a wider span, which explains the spreading of the ice/gas cloud observed by satellite (Fig. 17 in Corradini et al., 2016).~~

~~Although t~~Tephra dispersal simulations are commonly carried out using the field-based TGSD and assuming a constant average column height (or MER) for the entire duration of the paroxysmal phase (panel a in Fig. 7~~),~~). However, it is evident that eruption intensity varies substantially with time and consequently the column height (e.g. Scollo et al., 2014; 2015). To account for such variability, we discretized the eruption into a set of phases in consistency with i) the plume height observations from the remote sensing measurements (Corradini et al., 2016) and ii) the exit velocities ~~calculated~~ retrieved ~~through the L-band Doppler radar (~~by VOLDORAD-2B~~;~~ (Donnadieu et al., 2015; 2016; 2017). The improved simulation ~~procedure~~ scheme (panels b and c in Fig. 7) is achieved by coupling this discretization with the ARPAE or ERA-Interim databases and the Integrated TGSD or ~~the~~ Whole TGSD ~~for the ARPAE or the ERA-Interim databases~~, respectively, depending on the inversion purpose~~.~~.

3.3 Inversion modelling strategy

Simulation optimization is carried out to assess the ESP, and among them the TGSD, leading to the numerical reconstruction of the tephra loading and airborne ash mass dispersal. ~~by varying the i~~Input parameters in Table 2 were varied at constant steps within their ranges facing to the inherent non-uniqueness solution for assessment purposes (e.g. Anderson and Segall, 2013). ~~In our case, we started by~~Starting by ~~inverting~~ inverting the Integrated TGSD, we tested~~made of the weighted Field and Radar distributions. To solve the inverse problem presented above, we simulated the tephra loading using~~ each~~a~~ ~~TGSD given by a~~ weight~~ed~~ing average combination of the Field and Radar TGSDs, ranging from 100 wt% Field TGSD to 100 wt% Radar TGSD, with a step of 5 wt%. To select the best combination, we compared the tephra loadings computed at the sampled sites until we best-fit the field measurements.

Considering the simulations, we used the scheme described in Sect. 3.2 (panels b and c in Fig. 7), which implies a ~~constant~~ set of column height values (and hence the corresponding MERs) ~~given by the FPlume model~~ with the average exit velocity.

Therefore, neither the column height, the MER, nor the exit velocity were changed in each simulation. However, we inverted the plume parameters (i.e. α and β) from 0.05 to 0.15 and 0.05 to 1.0, respectively (Costa et al., 2016b), by means of the following goodness-of-fit procedure.

The goodness of ~~the~~ fit between simulations and field observations~~s~~ was evaluated through different statistical metrics (see Poret et al., 2017). In particular, we used the normalized Root Mean Square Error (i.e. *RMSE*) assuming 3 different error distributions (i.e. $RMSE_1$, $RMSE_2$, *and* $RMSE_3$) described in Folch et al. (2010). We also used~~for the tephra loadings and~~ the Aida (1978)'s indexes K (i.e. geometric average of the distribution) and k (i.e. geometric standard deviation of the distribution).

$$K = exp\left[\frac{1}{N}\sum_i^N \log\left(\frac{Obs_i}{Sim_i}\right)\right]$$

$$k = exp\left[\sqrt{\frac{1}{N}\sum_i^N \log\left(\frac{Obs_i}{Sim_i}\right)^2 - \left(\frac{1}{N}\sum_i^N \log\left(\frac{Obs_i}{Sim_i}\right)\right)^2}\right]$$

where i refers to the i^{th} sample over N, Sim and Obs are the simulated and observed tephra loadings, respectively. For a given set of ESPs, K gives the gap between the theoretical optimal tephra loading samples and the simulated ones. ~~-~~The reliability of the simulations is obtained for K between 0.95 and 1.05, which means a threshold of ±5 wt% from the derived theoretical optimal TEM~~ estimated on the basis of the tephra loading samples~~. It follows that the best simulations are selected for K close to 1 with k and the 3 *RMSEs* ~~at their~~ minim~~um~~ized. Additionally, we estimated the bias, the correlation, and the Student T test (Folch et al., 2010~~; Gouhier et al., Submitted~~).

After the Integrated TGSD, the Whole TGSD is inverted ~~Throughout the simulations, we used the eruption discretization (Sect. 3.2), implying a constant set of column height values, and hence, the corresponding MERs by means of the relationship (Folch et al., 2016). Each phase is achieved with the average exit velocity measured by VOLDORAD 2B. To overcome the non-uniqueness ESP combination, we worked on capturing the sampled tephra loadings by calibrating both the radial and cross-flow entrainment coefficients (α and β) from 0.05 to 0.15 and 0.05 to 1.0, respectively (Costa et al., 2016b).~~ by~~To account for the satellite retrievals, we used the Whole TGSD~~ quantitatively ~~exploring~~ analy~~s~~zing the effect of~~a large range of~~ different PM_{20} fractions (i.e. ~~from~~ 0.6 ~~to~~ 10.7 wt%; Sect. 3.1) ~~in order to~~on ~~best reproduce~~ the computed airborne ash dispersal. The ~~optimal~~ best fraction is ~~obtained~~ selected ~~through a quantitative comparison by means of~~by means of the following ~~three~~ 3 statistical metrics. ~~As first, w~~T~~e evaluated t~~he mass difference ~~in terms of mass~~ (i.e. $\Delta Mass$) between the satellite measurements and the FALL3D estimates. ~~To do so, w~~We compared the masses over the number of pixels given by the plume mask (obtained for the threshold of 0.1 t/km^2) retrieved from SEVIRI:

$$\Delta Mass = \frac{1}{\Delta T}\int_{t_0}^{t_f} (M_{Obs} - M_{Sim})\, dt \tag{3}$$

where M_{Obs} and M_{Sim} are the observed and simulated masses integrated over the whole event (i.e. from $t_0 = 09{:}30$ to $t_f = 14{:}30$, with $\Delta T = t_f - t_0$). This index gives the discrepancy (in tons) for each γ factor (i.e. PM_{20} fractions). Additionally, we also calculated for each γ factor the absolute average difference of mass per unit area ($\overline{Sum(\Delta)}$ in t/km^2) for the entire volcanic cloud by the following:

$$\overline{Sum(\Delta)} = \frac{1}{\Delta T}\int_{t_0}^{t_f} \frac{\sum_N |M_{Obs}(N) - M_{Sim}(N)|}{Area_P}\, dt \tag{4}$$

where N is the number of pixels (i.e. plume mask), $M_{Obs}(N)$ and $M_{Sim}(N)$ are the observed and modelled masses associated with the N^{th} pixel for SEVIRI and FALL3D, respectively. $Area_P$ refers to the area covered for the related time interval,

which is calculated by means of N and the pixel resolution (i.e. 9 km^2). This index ~~aims at indicating~~indicates the uncertainty of the simulated airborne ash mass per unit area with respect to the satellite ~~retrieved~~retrieval.

Considering that $\Delta Mass$ and $\overline{Sum(\Delta)}$ are discrepancy estimates, the selection is done on the basis of their minimization. Nonetheless, $\overline{Sum(\Delta)}$ gives absolute values preventing from any over- or under-estimation characterization. It follows that we evaluated also the following index:

$$\varepsilon = \frac{1}{\Delta T}\int_{t_0}^{t_f} \frac{[\sum_N M_{Obs}(N) - M_{Sim}(N) < 0] + [\sum_N M_{Obs}(N) - M_{Sim}(N) > 0]}{Area_P}\, dt \quad (5)$$

where ε refers to an over-estimation per pixel when $\varepsilon < 0$ and an under-estimation per pixel for $\varepsilon > 0$, with a best-fit for $\varepsilon = 0$. Moreover, the index indicates the average mass difference per unit area (i.e. t/km^2) between the satellite measurements and the simulation. The synergic use of these metrics aims at providing a ~~robust~~ simple way of comparing spatially and temporally the simulation outputs ~~and~~ with the field and remote system measurements.

4 Results and Discussion

T~~This~~ his section ~~first~~ describes the results of the inversion of i) the ESPs, and among them, ii) the Integrated TGSD ~~obtained in terms of best weights to use to obtain the Integrated TGSD~~ reproducing the tephra loading~~s~~. Then, iii) we report the results for assessing the PM_{20} fraction needed within the Whole TGSD to ~~reproduce~~ capture ~~both the tephra loadings and~~ the airborne ash transported in ~~the far~~ distal area~~field~~. ~~Beside the ESPs associated with the different TGSDs, we present the simulation results against field, ground-based and satellite measurements.~~

4.1 ESP inversion

~~The~~ Regarding the ~~inversion procedure initiated by estimating the~~ Integrated TGSD inversion (Sect. 3.3), ~~through the relative investigation of weighting factors for both the Field and Radar TGSDs. ing average~~The ~~corresponding~~ statistical analysis ~~(Table 2) shows~~for the best simulation (i.e. $K \approx 1$, $RMSE_1$, $RMSE_2$, $RMSE_3$, and k minimized) for each weighting average combination~~minimum values for *RMSEs* and *k* through a large range of combinations~~. Regardless of the weights, ~~Meanwhile, considering that the~~ $RMSE_1$ and $RMSE_3$ have flat patterns ~~through the weights~~, motivating we relied on the $RMSE_2$ and k. They show ~~selectable~~ relevant combinations from (65,35; i.e. 65 and 35 in wt% for the Field and Radar TGSDs respectively) to (85,15). Although $RMSE_2$ ranges between 1.56 to 1.85 from (65,35) to (85,15), k is minimized at 2.95 for (75,25), ~~motivat~~being ~~to~~ selected ~~this combination~~ as best weighting average combination ~~to~~ for ~~compose~~ composing the Integrated TGSD (Table ~~2~~ 3 and Fig. 8). It is worth noting that $RMSE_2$ and k indicate relatively high values yielding a mean error factor nearby 3, which is comparable to uncertainties associated with other classical methods (Bonadonna and Costa, 2012; 2013; Bonadonna et al., 2015).

~~To capture the main airborne ash dispersal feature retrieved from SEVIRI (displayed as animation A1 in the supplementary material), we carried out a quantitative comparison (Sect. 3.3) for different PM_{20} fractions (i.e. 0.6-10.7 wt%).~~ Figure 9 illustrates t~~T~~he statistical analysis of the Whole TGSD inversion (Sect. 3.3) for the best simulation for each ~~aims at selecting the correct amount of~~ PM_{20} ~~necessary to ensure the simulation of the ash dispersal~~fraction. ~~Figure 9 illustrates the inversion by showing the optimization of the statistical indexes.~~ Considering the whole airborne ash mass, the results yield a best value for $\Delta Mass$ at $\gamma = 0.65$ (i.e. PM_{20} = 9.0 wt%), indicating an overall under-estimation of ~76 tons of ash by FALL3D for the entire eruption. Then, $\overline{Sum(\Delta)}$ shows ~~a minima~~a minimum for $\gamma = 0.40$ (i.e. PM_{20} = 3.6 wt%), ~~which~~ give~~s~~ing an absolute average difference of mass per unit area of ~0.37 t/km^2 for the whole sequence. The third index returns a~~n~~ ~~optimal~~ best value of $\varepsilon = -0.03$ t/km^2 for $\gamma = 0.65$ (i.e. PM_{20} = 9.0 wt%), being consistent with $\Delta Mass$. ~~εThis index~~ likely reflects that

FALL3D slightly over-estimates the average mass per pixel of 0.03 t/km^2. ~~From the i~~By integrati~~on~~ng ~~of~~ the ~~statistical analysis~~ results (Fig. 9), the Whole TGSD required the minimum PM_{20} fraction of 3.6 wt% to best reproduce in absolute the average ash mass per unit area. However, such a fraction is not sufficient for best simulating the whole airborne ash mass released during the eruption, and minimizing the over- or under-estimation, which tends to be satisfied with higher PM_{20} fractions (i.e. 9.0 wt%). The corresponding input TGSD is displayed in Fig. 5. ~~In fact~~Moreover, $\Delta Mass$ and ε in Fig. 9 both indicate that FALL3D under-estimates substantially the airborne mass for PM_{20} fractions lower than ~7 wt% and over-estimates above ~10 wt%.

Regarding the ~~computational~~ other ~~parameterization~~ESPs, although the column height values were not changed ~~set accordingly to the direct monitoring and X-Radar observations. Considering the high time-dependent variability of the column height (Fig. 7)~~throughout the simulations (panels b and c in Fig. 7), we report here the MER inverted ~~through~~ by FPlume ~~is reported here~~ for the climax phase only, with is of ~7.0 × 10^5 kg/s. The calibration of ~~the air entrainment coefficients (~~α and β~~)~~ returns values ranging from 0.~~06~~ 06 ~~to~~ 0.15 and ~~from~~ 0.21 ~~to~~ 1.00, ~~for α and β,~~ respectively, depending on the weighting average combination (Table 3). ~~being~~The latter ranges are consistent with the literature (Devenish et al., 2010; Suzuki and Koyaguchi, 2015).

4.2 Tephra loading

During the ~~inversion of the~~ Integrated TGSD inversion, the 6 proximal samples were relatively stable when varying the weighting average combination~~s~~, whereas the farthest ~~measurement~~ sample (i.e. TER) was substantially affected. Figure 8 shows the comparison between the computed and measured ~~field~~ tephra loadings ~~and the computed values making use of~~with the Integrated TGSD (details in Table 1). It is worth noting that making use of the Field TGSD prevents FALL3D from capturing the TER ~~tephra loading~~sample, while the Radar TGSD fails on most of the samples as indicated ~~by the computed values~~ in Table 1. These observations argue the necessity ~~to~~ to ~~combine~~ combining the two different distributions through the Integrated TGSD, especially when field measurements are few. Figure 8 shows ~~Among t~~the 7 samples~~, all the proximal ones~~ lyinge within the 1/5- 5-times threshold of the measured tephra loadings, especially~~. T~~ the unique medial sample (i.e. TER) ~~is accurately computed with respect to the measurement (all tephra loadings detail is reported in Table 1)~~. As indicative values from Table 1, ~~Although~~ the 6 proximal ~~field measurement~~samples ~~(Table 1)~~ indicate tephra loadings ~~per unit area~~ ranging from 1 to 17 kg/m^2~~,~~. In contrast, FALL3D computed them between 3 and 7 kg/m^2 for the Integrated TGSD. Such ~~a lower span~~narrower range compared to the field ~~samples~~ data ~~is~~ can be attributed to the ~~higher difficulty~~ complexity for ~~the~~ modelling ~~to simulate in the very~~ proximal area (< 20 km from source), and~~. Additionally,~~ the field samples location ~~of the field samples~~ with respect to the main plume axis ~~also affects the resulting tephra loadings, especially at such proximal distance (less than 20 km from source)~~.

Besides the tephra loadings, we also compared ~~The~~ the field-derived ~~numerical results in terms of~~ GSD ~~related to~~at the sampled sites with the numerical results ~~obtained with~~for the Integrated TGSD ~~are compared with the field-derived ones~~ (see Fig. S1 in the supplementary material). ~~In fact, making use of the Integrated TGSD allows~~Although FALL3D ~~to~~ reproduces accurately 3 of the 7 samples by peaking at the same modes~~. However~~, 4 proximal samples (i.e. CRT, PDM, FFD and GDN) ~~have the mode~~are shifted by 1 Φ, ~~which~~ indicat~~es~~ing ~~that~~ the field measurements ~~are~~ being slightly finer than the computed ones. ~~As described~~ mentioned ~~above, t~~The~~is~~ discrepancy ~~is~~ argues~~related to~~ the difficulty for computing accurately at such proximal areas due to plume dynamic complexities (e.g. Cerminara et al., 2016). ~~Indeed, FPlume uses the TGSD to solve the mass conservation equation for each class distributing along the column. Then, the mass for each particle class at each level is transported laterally using FALL3D.~~ Nonetheless, the mode shift can also be attributed to the sampling distance from the source as explained in Spanu et al. (2016). Indeed, at proximal area the coarse ~~material~~ tephra (-4 ≥ Φ ≥ -2) is depositing rapidly, increasing the difficulty of estimating accurately this part of the TGSD ~~by means of~~with the Voronoi tessellation method together with a paucity of field measurements (Andronico et al., 2014). Moreover, we cannot exclude partial

breakages of few coarse-grained clasts when impacting the ground (Andronico et al., 2015), which also may result on grain-sizes slightly finer than expected.

Although ~~As described in Sect. 3.2,~~ we used the improved ~~the numerical description of the eruption phases accompanied by the input TGSD estimation, which aims at capturing both the tephra loading and airborne ash dispersal. Nonetheless~~simulation scheme (Sect. 3.2; panel b in Fig. 7), we run a simulation through the simplified procedure (panel a in Fig. 7) to highlight the ~~difference~~ effect on ~~in terms of~~the tephra loading, and therefore the statistical analysis ~~with the panel b (Fig. 7)~~. The ~~statistical analysis~~results ~~s~~ show ~~s~~ that making use of a constant plume height (here ~11.3 km a.s.l.) for the entire paroxysmal phase give ~~(here ~11.3 km a.s.l.) gives~~ K = 1.01 and k = 5.76 with $RMSE_1$ = 0.80, $RMSE_2$ = 3.36, and $RMSE_3$ = 1.33, which are significantly higher than for the improved procedure (~~panel b in Fig. 7 and~~ details in Table ~~2~~3). Regarding the TEM, the simplified scheme returns 1.5 × 10^9 kg, which is ~34 % higher than for the integrated approach with 1.2 × 10^9 kg. ~~In contrast, t~~The latter TEM is in good agreement with the estimation of 1.3 × 10^9 kg reported in Andronico et al. (2015). It is worth noting that~~,~~ varying the weighting ~~factors~~ average from 100 wt% Field TGSD towards 100 wt% Radar TGSD~~,~~ yields an increasing TEM going from 1 to 6 × 10^9 kg, respectively (Table ~~2~~3). This observation on TEM is consistent with the results described in Corradini et al. (2016), which indicates a X-Radar-derived total mass of 3.0 × 10^9 kg ~~retrieved from the radar~~ compared to the field-derived TEM of 1.3 × 10^9 kg ~~of~~ from Andronico et al. (2015). Such a difference between X-Radar and field-based TEM estimates ~~of the TEM~~ can be explained by considering the following aspects: i) X-Radar samples airborne particles during their fallout whereas the field measurements are based on deposited tephra; ii) the operative window focuses the X-Radar retrievals on detecting the ash particles (-1 to 5 Φ), while the field sampling method expands the measurements to block-sized (-5 to 5 Φ); iii) t~~T~~he Radar TGSD refers to the average over the duration observed from the radar at the sampled grid points, which not necessarily coincides with the duration and location characterized by the Field TGSD; iv) as explained in Sect. 3.1, the X-Radar measurements are made ~~by means of some~~with assumptions ~~and~~ using a regression model of radar simulations, which can add a further degree of uncertainty. The assumptions mainly affecting the final radar retrieval involve the radar forward model used to set up the radar retrieval scheme. It follows that assumptions made on particle shape, density, orientation, and PSD play the key role. However, the presented integrated approach by weighting the distributions issued from different methods aims at preventing the resulting Integrated TGSD from being associated with the full uncertainty of a single source.

The use of the different distributions (i.e. Field, Radar, Integrated, and Whole TGSDs) presented in this study permits comparing the resulting tephra loading maps (Fig. 10).~~To study the far-travelling airborne ash, we used the simulation procedure displayed on the panel c in Fig. 7, which refers to the wider computational domain (ERA Interim). Making use of the different TGSDs reported in this study, we produced the associated tephra loading maps in Fig. 10. Although the quantitative comparison was carried out by means of other statistical metrics than for the tephra loading validation (Sect. 3.3), the simulations were constrained in terms of tephra loading by converging towards the TEM computed through the Integrated TGSD with the ARPAE database. It results that t~~The tephra loading scale reported ~~on the following maps (~~in Fig. 10~~)~~ refers to the use of the ERA-Interim database, ~~indicates~~ indicating slightly different tephra loadings than the values in Table 1 (ARPAE) ~~(ERA-Interim)~~. ~~Indeed~~Here, Fig. 10 is used as indicative tephra loading maps to display the effect of the input TGSD on the resulting~~does not aim at comparing the tephra loading values at the sampled sites but is used in terms of whole~~ tephra dispersal, ~~validated~~ showing ~~by~~ the affected areas (e.g. Calabria and Puglia regions). In particular, ~~Making use of the different TGSDs reported in this study, we produced the associated tephra loading maps in Fig. 10. The figure aims at showing that by means of~~ the use of the Field TGSD (panel a) permits~~,~~ FALL3D ~~was able~~ to ~~simulate~~ compute the tephra loadings at the sampled sites up to Calabria, but not ~~the~~ in Puglia region~~,~~ where ash was reported. The Radar TGSD (panel b) operates in the ash window preventing its use from reproducing any tephra loading and airborne ash data. In contrast, the Integrated and Whole TGSDs (panels c and d) ~~both~~ capture all the tephra loading samples, but only the Whole

TGSD succeed on simulating the far-travelling airborne ash mass retrieved from satellite. The corresponding time-series animation of the tephra loading associated with the Whole TGSD is available as supplementary material (Animation A2).

4.3 Airborne ash dispersal

As mentioned in Sect. 2, ~~during the paroxysmal phase, the eruption released simultaneously~~ large quantities of ash, water vapour (transformed into ice) and SO_2 gas (Fig. 4) were released from Etna, preventing the remote systems from ~~observing and~~ quantifying the whole event easily. ~~In our case, t~~The formation of two volcanic clouds (AC and IC) following ~~two~~ their own ~~different~~ trajectory~~ies~~ at different ~~their own~~ altitudes (~~i.e. ~ 6 km for AC and ~ 11 km for IC;~~ Fig. 3) increased substantially the complexity of comparing quantitatively the far-travelling airborne ash masses (i.e. SEVIRI and FALL3D). Indeed, the columnar satellite measurements and FALL3D results prevent from isolating the two clouds, which motivated this study to focus on the plume mask retrieved by SEVIRI for each time (Fig. 11). ~~The f~~Figure ~~aims at~~11 ~~illustrating~~ illustrates the ~~quantitative~~ comparison ~~carried out~~ between the ~~observed~~ retrieved and computed airborne ash mass ~~at each time interval. Considering the inversion of the PM_{20} fraction reported above (Sect. 4.1)~~ By means of the inverted PM_{20} range (i.e. 3.6-9.0 wt%), w~~, w~~e displayed the airborne ash mass maps ~~related to the optimal range of PM_{20}. Indeed, t~~The left column refers to the minimum PM_{20} fraction (i.e. 3.6 wt%) required to capture accurately the absolute average difference of mass per unit area (i.e. $\overline{Sum(\Delta)}$), whereas the right column corresponds to the fraction (i.e. 9.0 wt%) best reproducing the whole airborne ash mass (i.e. $\Delta Mass$ and ε). ~~As example, e~~Each panel in Fig. 11 shows the overlapping ~~of~~ between the SEVIRI retrievals ~~with~~ and the FALL3D outputs for a given time. Although the overlap tends to decrease with time, the results ~~related to~~for $\gamma = 0.65$ (i.e. PM_{20} = 9.0 wt%) indicate a better performance than for ~~at~~ $\gamma = 0.40$ (i.e. PM_{20} = 3.6 wt%). The entire time-series animations are available in the supplementary material (~~animations~~ Animations A3 and A4 for $\gamma = 0.40$ and $\gamma = 0.65$, respectively).

~~-~~The ~~reported~~ PM_{20} ~~fraction~~ range obtained for the 23rd November 2013 Etna paroxysm ~~is~~ tends to be relatively high with respect to the literature (1-2 wt%; Corradini et al., 2016), ~~which can be~~eventually attributed to the observational data used and the instrument properties. However, in terms of mass to the TEM, the estimated PM_{20} fractions indicate consistent values. Indeed, 1-2 wt% of the X-Radar TEM (3.0×10^9 kg) refers to 30-60 tons, while 3.6-9.0 wt% of the integrated TEM (1.2×10^9 kg) gives 43-108 tons. In fact, Corradini et al. (2016) integrated X-Radar data with satellite retrievals to assess the PM_{20} fraction. However, the satellite ~~does~~ cannot ~~allow any~~ quantifi~~cationy of~~ any ash mass from pixels mainly filled by ice or gas (e.g. SO_2). In other words, although the volcanic ice/gas clouds (i.e. IC) are assumed to be produced from ash nucleus (Corradini et al., 2016), the probable presence of ash within such clouds will be missed from SEVIRI.

Being the airborne ash mass spreading downwind towards the far-field, the very fine ash fraction (i.e. here 3.6-9.0 wt% of the erupted mass) is a critical input into operational tephra dispersal models (e.g. HYSPLIT, Stunder et al., 2007; NAME, Witham et al., 2007; FALL3D, Folch et al, 2012), which are widely used for aviation safety~~airborne ash~~. Although few studies have attempted to better constrain the fraction estimation, eruptions from different volcanoes are not comparable as ~~the~~ such a fraction ~~of very fine ash~~ is very different from one case to the other, ranging from 50 wt% to few wt% (Rose and Durant, 2009). As discussed by Costa et al., (2016a; 2017), the very fine ash fraction varies with eruption intensity~~, and~~ magma composition, and eruption style. In particular, at the Spurr 1992's eruption, Wen and Rose (1994) estimated ~2 wt% dispersed into the distal area. At the Eyjafjallajökull 2010's eruption, the estimated range span from ~0.9-11 wt% (Bonadonna et al., 2011; Dacre et al., 2011; Devenish et al., 2012). However, ~~tThe fact that Hysplit or other~~some operational models assume a fraction of ~~~about~~ 5 wt%, which is not related with ~~what we~~our estimate for the Etna eruption. ~~In the former case~~As discussed by Costa et al., (2016; 2017) such a fraction is not constant but vary with eruption intensity and magma composition. ~~For the operational model a~~In fact, assuming a constant fraction~~,~~ (e.g. 5 wt%) would represent the very fine ash fraction that escapes to aggregation processes and travels in the far field. In the case of basaltic eruptions, like ~~for the case of~~at Etna, the eruption intensity and the very fine ash content are ~~is~~ low~~er~~, and hence aggregation less efficient

(Costa et al., 2010), implying that ~~almost all the~~most of the ~~very fine ash~~ fraction can be transported distally. These observations yield the necessity for better considering such fraction as input, suggesting further investigations on both basaltic and silicic volcanoes.

Regarding the FALL3D results in ~~Figure~~ Fig. 11, ~~also~~ the airborne ash maps ~~indicates the presence of~~show the two volcanic clouds (AC and IC) observed from satellite (Corradini et al., 2016), although ~~in our case~~ they are still connected to each other. ~~Although they d~~Dispersed~~ed~~ing simultaneously from the source, the FALL3D simulations yield the presence of volcanic ash following the trajectory of AC below FL 250. In addition, FALL3D also indicates a major contribution of the airborne mass associated with the IC trajectory spreading over FL 250. The ~~numerical~~ results in terms of temporal dispersal (Animation A3) are corroborated by the SEVIRI ~~observations~~ retrievals (Animation A1) and the pilot report, which mentioned volcanic ash and probably gas near Albania at FL 360-380 (Crompton and Husson, 2015).

As a consequence of being blind to any ash within the IC, the comparative study~~, the~~ results ~~reported above~~ represent partially the whole airborne ash. ~~Indeed, only the AC was investigated quantitatively, whereas the IC was just observed.~~ This raises questions related to volcanic hazards, such as the air traffic safety. In fact, on the basis of the FALL3D results, the IC appears to have a significant amount of erupted material (i.e. PM_{20}, ice and gas). This observation highlights the necessity for quantifying entirely the far-travelling airborne ~~erupted material~~tephra, perhaps benefitting from other sensors capable to characterize such aerosol clouds. In particular, this study inferred from quantitative ~~studies~~ analysis based on the observations in terms of tephra loading and airborne ash mass the interest for integrating retrievals from diverse instruments to assess accurately the initial magma fragmentation (i.e. TGSD of the whole erupted tephra).

5 Conclusions

Recent studies have shown the need for improving the assessment of the eruption source parameters to reduce the uncertainties and present more realistic numerical outputs, which can be used for hazards mitigation. Here, we worked on better estimating the initial magma fragmentation (i.e. Total Grain-Size Distribution – TGSD) by integrating measurements from field samples, ground-based (X-band weather radar) and satellite-based (SEVIRI) systems. We applied the methodology ~~on~~ to the 23rd November 2013 Etna paroxysm, which benefited from north-easterly wind directions~~s~~ that dispersed the tephra over the Calabria towards the Puglia (Italy) and Albania regions. The available observations in terms of tephra loadings and airborne ash dispersal were used to reconstruct numerically (through the FALL3D model) the eruption features from the source to distal areas. In fact, the field-based TGSD reproduces only the sampled tephra loadings, whereas the Radar TGSD refers to a limited range of ash classes preventing its use within FALL3D as initial TGSD. We produced ~~a~~ an ~~weighted~~ Integrated TGSD (i.e. ~~weighted~~ weighting average of field + radar distributions) to best-fit the tephra loadings. The inversion results yield a TGSD made of 75 wt% of the Field TGSD and 25 wt% of the Radar TGSD. However, the Integrated TGSD does not account for the far-travelling airborne ash mass ~~observable~~ retrieved from satellite (i.e. PM_{20}). ~~To do so, w~~We empirically modified the Integrated TGSD to implement the SEVIRI retrievals by investigating diverse PM_{20} fractions (i.e. 0.6-10.7 wt%), until we best-fit the measurements. The inverted PM_{20} fraction best-matching the ~~satellite observations~~SEVIRI data ~~appears to~~ ranges from 3.6 ~~to~~ -9.0 wt%, depending on capturing the whole airborne ash mass or the mass per unit area. ~~Although the these results~~sing ~~in terms of PM_{20} fraction range suggests larger values than that reported by Corradini et al. (2016), they reflect the required fractions we to used within the input TGSD for best reproducing the satellite retrievals. In fact, t~~The~~is~~ study highlighted the ~~necessity~~ need for improving the integration of data from different instruments ~~together with the~~to better ~~quantification~~ quantify ~~of the~~ tephra loading and ~~the~~ airborne mass (i.e. PM_{20}, ice, and gas), especially when aerosol clouds are produced during the eruption. ~~The TEM related to the Whole TGSD is estimated at 1.2×10^9 kg.~~ From a computational point of view, the assessment of the initial TGSD would benefit from such integration, being ~~This study illustrated the need for integrating the observations from different instrument to achieve a better estimate of~~

~~the initial TGSD~~ widely used for mode~~l~~lling purposes such as for air traffic safety. This work aims at being of interest for developing new methods or tools capable to assess the full size-spectrum TGSD ~~covering entirely the grain size spectrum~~. ~~As indicative results, TEM is estimated at 1.2×10^9 kg.~~

Supplement

The supplement associated with this manuscript serves for illustrating the results in terms of individual grain-size distributions ~~related to the use of~~with the Integrated TGSD, which is validated on the basis of the tephra samples (Fig. S1). ~~Then, t~~The time-series animations aim at highlighting the main eruption features (i.e. whole tephra loading and airborne ash dispersal) ~~associated with the use of different input TGSDs~~.

Figure S1

Comparison of the 7 ~~-~~ individual~~s~~ field-derived GSDs with the computed ones through the FALL3D model. The figure indicates the reproducibility of the local GSD by peaking at the ~~correct~~ same mode. The shifted GSDs are discussed in Sect. 4.2.

Animation A1

The time-series animation refers to the dynamic evolution of the volcanic ash cloud travelling from the source retrieved from SEVIRI (i.e. 09:30-14:30 UTC).

Animation A2

The time-series animation corresponds to the simulation of the tephra loading obtained for the Whole TGSD with ~~the empirical~~ $\gamma = 0.65$ ~~factor of 0.65~~. The animation shows the ~~dynamic~~ temporal expansion of the tephra fallout indicating the affected areas (i.e. 09:30-14:30 UTC).

Animation A3

The time-series animation shows the simulation of the airborne ash dispersal associated with the Whole TGSD produced with $\gamma = 0.40$ (i.e. 09:30-14:30 UTC). This animation indicates the ~~dynamic~~ temporal dispersal ~~associated with~~obtained with the initial injection of 3.6 wt% of PM_{20} into the atmosphere. ~~It indicates the presence of a~~The major lobe ~~going~~ goes towards Albania, which corresponds to the ice/gas volcanic cloud, whereas the minor lobe (i.e. tail) ~~is~~ spread~~ings~~ towards the Puglia region (southern Italy) and is related to the volcanic ash cloud.

Animation A4

The time-series animation is referring to the simulation of the far-travelling airborne ash dispersal computed with the Whole TGSD for ~~the~~ $\gamma = 0.65$ (i.e. 09:30-14:30 UTC). This animation shows a similar dispersal than for the Animation A3. However, ~~making~~ using ~~use of~~ $\gamma = 0.65$ means the initial injection of 9.0 wt% of PM_{20} into the atmosphere, which results on higher ash mass values, especially for the major lobe spreading towards Albania.

Author contribution

M. Poret conceived the idea and defined the project approach together with ~~the~~ A. Costa, S. Corradini, and L. Merucci. M. Poret and A. Costa compiled the FALL3D simulations and co-wrote the manuscript. S. Corradini and L. Merucci provided and processed the SEVIRI data. G. Vulpiani and M. Montopoli provided and processed the X-band weather radar data. D. Andronico provided and processed the field data. V. Freret-Lorgeril provided and processed the L-band VOLDORAD 2B data. All the co-authors work on the interpretation of the results and finalization of the manuscript.

Competing interests

The authors declare no conflict of interest.

Acknowledgment

MP received the funding from the FP7 Marie Curie Actions Framework "FP7-PEOPLE-2013-ITN", project VERTIGO grant number 607905. AC and DA acknowledges the European project EUROVOLC (grant number 731070) and the MIUR project Premiale Ash-RESILIENCE. The ERA-Interim Reanalysis meteorological database was retrieved from the European Center for Medium-Range Weather Forecasts (ECMWF) and the ARPAE database from the INGV-OE archives. The L-band Doppler radar (VOLDORAD 2B) data were provided by the open-access database on the OPGC website: http://voldorad.opgc.fr/. The radar is operated jointly by the OPGC and INGV-OE (Catania, Italy) in the framework of a collaboration agreement between INGV-OE, the French CNRS and the OPGC-Université Clermont Auvergne in Clermont-Ferrand (France). The X-band weather radar data were provided by the Civil Protection Department (Rome, Italy) and the MSG-SEVIRI data by the INGV in Rome. We are also grateful to Boris Behncke (INGV–OE) for the imagery support ~~related~~ of ~~to~~ the eruption. We also warmly acknowledge M. Cantanero, R.A. Corsaro, and A. Cristaldi who helped to collect the tephra samples and ~~analyse~~analys~~z~~e them. Finally, we are grateful to L. Mastin and an anonymous reviewer for their valuable comments that improved the quality and clarity of the manuscript.

References

1. Aida, I.: Reliability of a tsunami source model derived from fault parameters. J. Phys. Earth, 26, 57–73, 1978.
2. Alparone, S., Andronico, D., Lodato, L., and Sgroi, T.: Relationship between tremor and volcanic activity during the Southeast Crater eruption on Mount Etna in early 2000. J. Geophys. Res., 108, B5, 2241. doi:10.1029/2002JB001866, 2003.
3. Anderson, K., and Segall, P.: Bayesian inversion of data from effusive volcanic eruptions using physics-based models: Application to Mount St. Helens 2004-2008, J. Geophys. Res. – Solid Earth, 118, 2017–2037. doi:10.1002/jgrb.50169, 2013.
4. Andronico, D., Scollo, S., Cristaldi, A., and Lo Castro, M.D.: Representivity of incompletely sampled fall deposits in estimating eruption source parameters: a test using the 12–13 January 2011 lava fountain deposit from Mt. Etna volcano, Italy, Bull. Volcanol., 76, 861. doi:10.1007/s00445, 2014.
5. Andronico, D., Scollo, S., and Cristaldi, A.: Unexpected hazards from tephra fallouts at Mt. Etna: The 23 November 2013 lava fountain, J. Volcanol. Geotherm. Res., 304, 118-125. doi:10.1016/j.jvolgeores.2015.08.007, 2015.
6. Andronico, D., and Del Carlo, P.: PM_{10} measurements in urban settlements after lava fountain episodes at Mt. Etna, Italy: Pilot test to assess volcanic ash hazard on human health, Nat. Hazards Earth Syst. Sci., 16, 29–40, 2016.
7. Barsotti, S., Neri, A., and Scire, J.: The VOL-CALPUFF model for atmospheric ash dispersal. I. Approach and physical formulation, J. Geophys. Res., 113, B03208. doi:10.1029/2006JB004623, 2008.
8. Behncke, B., Branca, S., Corsaro, R.A., De Beni, E., Miraglia, L., and Proietti, P.: The 2011–2012 summit activity of Mount Etna: birth, growth and products of the new SE crater, J. Volcanol. Geotherm. Res., 270, 10–21. doi:10.1016/j.jvolgeores.2013.11.02, 2014.
9. Beckett, F.M., Witham, C.S., Hort, M.C., Stevenson, J.A., Bonadonna, C., and Millington, S.C.: Sensitivity of dispersion model forecasts of volcanic ash clouds to the physical characteristics of the particles, J. Geophys. Res. – Atmos., 120. doi:10.1002/2015JD023609, 2015.
10. Bonaccorso, A., Calvari, S., Linde, A., and Sacks, S: Eruptive processes leading to the most explosive lava fountain at Etna volcano: The 23 November 2013 episode, Geophys. Res. Lett., 41, 4912–4919, doi:10.1002/2014GL060623, 2014.
11. Bonadonna, C., and Houghton, B.F.: Total grain-size distribution and volume of tephra-fall deposits, Bull. Volcanol., 67, 441–456. doi:10.1007/s00445-004-0386-2, 2005.

12. Bonadonna, C, Genco, R, Gouhier, M, Pistolesi, M, Cioni, R, Alfano, F, Hoskuldsson, A, and Ripepe, M.: Tephra sedimentation during the 2010 Eyjafjallajeökull eruption (Iceland) from deposit, radar, and satellite observations, J. Geophys. Res. – Solid Earth. doi:10.1029/2011JB008462, 2011.
13. Bonadonna, C., and Costa, A.: Estimating the volume of tephra deposits: a new simple strategy, Geology, 40, 415–418. doi.org/10.1130/G32769.1, 2012.
14. Bonadonna, C., and Costa, A.: Plume height, volume, and classification of explosive volcanic eruptions based on the Weibull function, Bull. Volcanol., 75, 742. doi:10.1007/s00445-013-0742-1, 2013.
15. Bonadonna, C., Biass, S., and Costa, A.: Physical characterization of explosive volcanic eruptions based on tephra deposits: Propagation of uncertainties and sensitivities analysis, J. Volcanol. Geotherm. Res., 296, 80–100. doi:10.1016/j.jvolgeores.2015.03.009, 2015.
16. Bursik, M.: Effect of wind on the rise height of volcanic plumes, Geophys. Res. Lett., 28, 3621–3624. doi:10.1029/2001GL013393, 2001.
17. Byun, D., and Schere, K. L.: Review of the governing equations, computational algorithms, and other components of the Models-3 Community Multiscale Air Quality (CMAQ) modeling system. Applied Mechanics Reviews, 59, 51–77. doi:10.1115/1.2128636, 2006.
18. Carbone, D., Zuccarello, L., Messina, A., Scollo, S., and Rymer, H.: Balancing bulk gas accumulation and gas output before and during lava fountaining episodes at Mt. Etna, Sci. Rep. 5, 18049. doi:10.1038/srep18049, 2015.
19. Cerminara, M., Esposti Ongaro, T., and Neri, A.: Large eddy simulation of gos-particle kinematic decoupling and turbulent entrainment in volcanic plumes. J. Volcanol. Geotherm. Res., 326, 143–171, doi:10.1016/j.jvolgeores.2016.06.018, 2016.
20. Corradini, S., Montopoli, M., Guerrieri, L., Ricci, M., Scollo, S., Merucci, L., Marzano, F. S., Pugnaghi, S., Prestifilippo, M., Ventress, L., Grainger, R. G., Carboni, E., Vulpiani, G., and Coltelli, M.: A multi-sensor approach for the volcanic ash cloud retrievals and eruption characterization, Remote Sensing – Special Issue on Volcano Remote Sensing, 8(1), 58. doi:10.3390/rs8010058, 2016.
21. Costa, A., Macedonio, G., and Folch, A.: A three-dimensional Eulerian model for transport and deposition of volcanic ashes, Earth Planet. Sci. Lett., 241, 634–647. doi:10.1016/j.epsl.2005.11.019, 2006.
22. Costa, A., Folch, A., and Macedonio, G.: A model for wet aggregation of ash particles in volcanic plumes and clouds: 1. Theoretical formulation. J. Geophys. Res., 115, B09201. doi:10.1029/2009JB007175, 2010.
23. Costa, A., Folch, A., and Macedonio, G.: Density-driven transport in the umbrella region of volcanic clouds: implications for tephra dispersion models. Geophys. Res. Lett., 40, 4823–4827. doi:10.1002/grl.50942, 2013.
24. Costa, A., Pioli, L., and Bonadonna, C.: Corrigendum to "Assessing tephra total grain-size distribution: Insights from field data analysis". (*Earth and Planetary Sci. Lett.* 443, 90–107, 2016); Earth and Planetary Sci. Lett., doi:10.1016/j.epsl.2017.03.003, 2017.
25. Costa, A., Pioli, L., and Bonadonna, C.: Assessing tephra total grain-size distribution: Insights from field data analysis, Earth and Planetary Sci. Lett., 443, 90–107, 2016a.
26. Costa, A., Suzuki, Y.J., Cerminara, M., Devenish, B., Esposti Ongaro, T., Herzog, M., Van Eaton, A., Denby, L.C., Bursik, M., de Michieli Vitturi, M., Engwell, S., Neri, A., Barsotti, S., Folch, A., Macedonio, G., Girault, F., Carazzo, G., Tait, S., Kaminski, E., Mastin, L., Woodhouse, M., Phillips, J.C., Hogg, A.J., Degruyter, W.J., and Bonadonna, C.: Results of the eruption column model inter-comparison study, J. Volcanol. Geotherm. Res. doi:10.1016/j.jvolgeores.2016.01.017, 2016b.
27. Crompton, E., and Husson, P.: Volcanic Ash Advisories: how the VAACs use the 'Discernible Ash' definition to draw their lines now and in the future, 7th International Workshop on Volcanic Ash (IWVA/7), Anchorage (Alaska), USA, 19–23 October, 2015. https://www.wmo.int/aemp/sites/default/files/P-09_Crompton-Husson.pdf

28. Dacre, H.F., Grant, A.L.M., Hogan, R.J., Belcher, S.E., Thomson, D.J., Devenish, B., Marenco, F., Haywood, J., Ansmann, A., and Mattis, I.: The structure and magnitude of the ash plume during the initial phase of the Eyjafjallajökull eruption, evaluated using lidar observations and NAME simulations, J. Geophys. Res., 116, D00U03. doi:10.1029/2011JD015608, 2011.

~~28.~~29. De Beni, E., Behncke, B., Branca, S., Nicolosi, I., Carluccio, R., D'Ajello Caracciolo, F., and Chiappini, M.: The continuing story of Etna's New Southeast Crater (2012-2014): Evolution and volume calculations based on field surveys and aerophotogrammetry, J. Volcanol. Geotherm. Res., 303, 175–186. doi:10.1016/j.jvolgeores.2015.07.021, 2015.

~~29.~~30. Degruyter, W., and Bonadonna, C.: Improving on mass flow rate estimates of volcanic eruptions, Geophys. Res. Lett., 39, L16308. doi:10.1029/2012GL052566, 2012.

31. Devenish, B. J., Rooney, G.G., Webster, H.N., and Thomson, D.J.: The entrainment rate for buoyant plumes in a crossflow, Boundary-Layer Meteorol. 134, 411–439, doi: 10.1007/s10546-009-9464-5, 2010.

~~30.~~32. Devenish, B., Francis, P.N., Johnson, B.T., Sparks, R.S.J., and Thomson, D.J.: Sensitivity analysis of dispersion modeling of volcanic ash from Eyjafjallajökull in May 2010, J. Geophys. Res., 117(D00U21). doi:10.1029/2011JD016782, 2012.

~~31.~~33. Donnadieu F., Freville P., Rivet S., Hervier C., and Cacault P.: The Volcano Doppler radar data base of Etna (VOLDORAD 2B), Université Clermont Auvergne – CNRS. http://wwwobs.univ-bpclermont.fr/SO/televolc/voldorad/bddtr.php. doi:10.18145/VOLDORAD.ETNA.2009, 2015.

~~32.~~34. Donnadieu F., Freville P., Hervier C., Coltelli M., Scollo S., Prestifilipo M., Valade S., Rivet S., and Cacault P.: Near-source Doppler radar monitoring of tephra plumes at Etna, J. Volcanol. Geotherm. Res., 312:26–39, 2016.

35. Donnadieu, F., Freret-Lorgeril, V., Coltelli, M., Scollo, S., Gouhier, M., Fréville, P., Hervier, C., and Prestifilippo, M.: Lava fountaining paroxysms generating tephra plumes at Mt. Etna: Remote sensing retrievals, IAVCEI meeting, Portland, 14-18 August 2017, USA, Poster VO43A-139.

~~33.~~36. Folch, A., Cavazzoni, C., Costa, A., Macedonio, G.: An automatic procedure to forecast tephra fallout, J. Volcanol. Geotherm. Res., 177, 767-777, doi:10.1016/j.jvolgeores.2008.01.046, 2008.

~~34.~~37. Folch, A., Costa, A., and Macedonio, G.: FALL3D: A computational model for transport and deposition of volcanic ash, Comp. Geosci., 35, 1334–1342. doi:10.1016/j.cageo.2008.08.008, 2009.

~~35.~~38. Folch, A., Costa, A., Durant, A., and Macedonio, G.: A model for wet aggregation of ash particles in volcanic plumes and clouds: 2. Model application, J. Geophys. Res., 115, B09202. doi:10.1029/2009JB007176, 2010.

~~36.~~39. Folch, A.: A review of tephra transport and dispersal models: Evolution, current status, and future perspectives, J. Volcanol. Geotherm. Res., 235–236, 96–115. doi: 10.1016/j.volgeores.2012.05.020, 2012.

~~37.~~40. Folch, A., Costa, A., and Basart, S.: Validation of the FALL3D ash dispersion model using observations of the 2010 Eyjafjallajökull volcanic ash clouds, Atmos. Env., 48, 165–183. doi:10.1016/j.atmosenv.2011.06.072, 2012.

~~38.~~41. Folch, A., Costa, A., and Macedonio, G.: FPLUME-1.0: An integral volcanic plume model accounting for ash aggregation, Geosci. Model Dev., 9, 431–450. doi:10.5194/gmd-9-431-2016, 2016.

~~39.~~42. Freret-Lorgeril, V., Donnadieu, F., Coltelli, M., Scollo, S., Fréville, P., Hervier, C., and Prestifilippo, M.: Doppler radar retrievals from lava fountaining paroxysms generating tephra plumes at Mt. Etna, EGU General Assembly, Vienna, 23-28 April, Poster,2016.

~~40.~~43. Ganser, G.H.: A rational approach to drag prediction of spherical and non-spherical particles. Powder Technol., 77, 143–152. doi:10.1016/0032-5910(93)80051-B, 1993.

~~41. Gouhier, M., Eychenne, J., Azzaoui, N., Guillin, A., Deslandes, M., Poret, M., Costa, A., and Husson, P.: Low efficiency of large volcanic eruptions in transporting fine ash into the atmosphere, Nature – Geosciences, submitted.~~

42.44. Guffanti, M., Casadevall, T.J., and Budding, K.: Encounters of Aircraft with Volcanic Ash Clouds: A Compilation of Known Incidents, 1953-2009. U.S. Geological Survey Data Series 545, ver. 1.0, 12 p., plus 4 appendixes including the compilation database, available only at http://pubs.usgs.gov/ds/545, 2010.

43.45. Horwell, C.J., Sargent, P., Andronico, D., Lo Castro, M.D., Tomatis, M., Hillman, S.E., Michnowicz, S.A.K., and Fubini, B.: The iron-catalysed surface reactivity and health-pertinent physical characteristics of explosive volcanic ash from Mt. Etna, Italy, J. Appl. Volcanol. doi:10.1186/s13617-017-0063-8, 2017.

44.46. Kaminski, E., Tait, S., and Carazzo, G.: Turbulent entrainment in jets with arbitrary buoyancy, J. Fluid Mech., 526, 361–376. doi:10.1017/S0022112004003209, 2005.

45.47. Macedonio, G., Costa, A., and Folch, A.: Uncertainties in volcanic plume modelling: A parametric study using FPlume, J. Volcanol. Geotherm. Res., 326, 92–102. doi:10.1016/j.jvolgeores.2016.03.016, 2016.

46.48. Mastin, L.G., Guffanti, M., Servranckx, R., Webley, P., Barsotti, S., Dean, K., Durant, A., Ewert, J. W., Neri, A., Rose, W.I., Schneider, D., Siebert, L., Stunder, B., Swanson, G., Tupper, A., Volentik, A., and Waythomas, C.F.: A multidisciplinary effort to assign realistic source parameters to models of volcanic ash-cloud transport and dispersion during eruptions, J. Volcanol. Geotherm. Res., 186, 10-21, 2009.

47.49. Montopoli, M.: Velocity profiles inside volcanic clouds from three-dimensional scanning microwave dual-polarization Doppler radars, J. Geophys. Res. – Atmos., 121. doi:10.1002/2015JD023464, 2016.

48.50. Morton, B.R., Taylor, G.I., and Turner, J.S.: Turbulent gravitational convection from maintained and instantaneous source, Phil. Trans. Royal Society, London, A 234, 1–23, 1956.

49.51. Poret, M., Costa, A., Folch, A., and Martì, A.: Modelling tephra dispersal and ash aggregation: The 26th April 1979 eruption, La Soufrière St. Vincent, J. Volcanol. Geotherm. Res, 347C, 207–220. doi:10.1016/j.jvolgeores.2017.09.012, 2017.

~~50. Poret, M., Costa, A., Andronico, D., Scollo, S., Gouhier, M., and Cristaldi, A.: Modelling eruption source parameters by integrating field, ground based and satellite based measurements: The case of the 23rd February 2013 Etna paroxysm, J. Geophys. Res – Solid Earth, submitted.~~

51.52. Prata, A.J., and Kerkmann, J.: Simultaneous retrieval of volcanic ash and SO_2 using MSG-SEVIRI measurements. Geophys. Res. Lett. 34, L05813. doi:10.1029/2006GL028691, 2007.

52.53. Rose, W.I., and Durant, A.J.: Fine ash content of explosive eruptions, J. Volcanol. Geoth. Res. doi:10.1016/j.jvolgeores.2009.01.010, 2009.

53.54. Scollo, S., Folch, A., and Costa, A.: A parametric and comparative study of different tephra fallout models. J. Volcanol. Geoth. Res. 176, 199–211. doi: 10.1016/j.jvolgeores.2008.04.002, 2008.

54.55. Scollo, S., Prestifilippo, M., Pecora, E., Corradini, S., Merucci, L., Spata, G., and Coltelli, M.: Eruption column height estimation of the 2011-2013 Etna lava fountains, Annals of Geophys., 57, 2, S0214. doi:10.4401/ag-6396, 2014.

55.56. Scollo, S., Boselli, A., Coltelli, M., Leto, G., Pisani, G., Prestifilippo, M., Spinelli, N., and Wang, X.: Volcanic ash concentration during the 12 August 2011 Etna eruption, Geophys. Res. Lett., 42. doi:10.1002/2015GL063027, 2015.

56.57. Spanu, A., Vitturi, M. dé M., and Barsotti, S.: Reconstructing eruptive source parameters from tephra deposit: a numerical study of medium-sized explosive eruptions at Etna volcano, Bull. Volcanol., 78, 59. doi:10.1007/s00445-016-1051-2, 2016.

58. Spilliaert, N., Allard, P., Metrich, N., and Sobolev, A.V.: Melt inclusion record of the conditions of ascent, degassing, and extrusion of volatile-rich alkali basalt during the powerful 2002 flank eruption of Mount Etna (Italy), J. Geophys. Res., 111, B04203. doi:10.1029/2005JB003934, 2006.

59. Stunder, B., Heffter, J.L., and Draxler, R.R.: Airborne volcanic ash forecast reliability, Weather and Forecasting, 22, 1132-1139, 2007.

~~57.~~60. Sulpizio, R., Folch, A., Costa, A., Scaini, C., Dellino, P.: Hazard assessment of far-range volcanic ash dispersal from a violent Strombolian eruption at Somma-Vesuvius volcano, Naples, Italy: Implications on civil aviation, Bull. Volc., 74, 2205-2218, doi:10.1007/s00445-012-0656-3, 2012.

~~58.~~61. Suzuki, Y.J., and Koyaguchi, T.: A three-dimensional numerical simulation of spreading umbrella clouds, J. Geophys. Res., 114, B03209. doi:10.1029/2007JB005369, 2009.

~~59.~~62. Suzuki, Y., and Koyaguchi, T.: Effects of wind on entrainment efficiency in volcanic plumes, J. Geophys. Res. – Solid Earth, 61, 6122–6140. doi:10.1002/2015JBO12208, 2015.

~~60.~~63. Tomašek, I., Horwell, C.J., Damby, D.E., Barošová, H., Geers, C., Petri-Fink, A., Rothen-Rutishauser, B., and Clift, M.J.D.: Combined exposure of diesel exhaust particles and respirable Soufrière Hills volcanic ash causes a (pro-) inflammatory response in an in vitro multicellular epithelial tissue barrier model, Particle and Fibre Toxicology, 13 (1), 67. doi:10.1186/s12989-016-0178-9, 2016.

~~61.~~64. Ulke, A.G.: New turbulent parameterization for a dispersion model in atmospheric boundary layer. Atmos. Environ., 34, 1029–1042, 2000.

65. Vulpiani, G., Ripepe, M., and Valade, S.: Mass discharge rate retrieval combining weather radar and thermal camera observations, J. Geophys. Res. – Solid Earth, 121, 5679–5695. doi:10.1002/2016JB013191, 2016.

66. Wen, S., and Rose, W.I.: Retrieval of sizes and total masses of particles in volcanic clouds using AVHRR bands 4 and 5, J. Geophys. Res., 99(D3), 5421-5431, 1994.

~~62.~~67. Witham, C.S., Hort, M.C., Potts, R., Servranckx, R., Husson, P., and Bonnardot, F.: Comparison of VAAC atmospheric dispersion models using the 1 November 2004 Grimsvötn eruption, Meteorol. Appl., 14, 27-38. doi:10.1002/met.3, 2007.

~~63.~~68. Woodhouse, M.J., Hogg, A.J., Phillips, J.C., and Sparks, R.S.J.: Interaction between volcanic plumes and wind during the 2010 Eyjafjallajökull eruption, Iceland, J. Geophys. Res. – Solid Earth, 118, 92–109. doi:10.1029/2012JB009592, 2013.

Tables

Table 1: Field measurements compared with the computed tephra loadings

Field observations						Computed loading (kg/m^2)			
Sample	Location	Longitude	Latitude	Mode (Φ)	Loading (kg/m^2)	Field TGSD	Radar TGSD	Integrated TGSD	Whole TGSD
CTL	Citelli	15.060	37.765	-3	1.7×10^{1}	7.2×10^{0}	3.4×10^{-1}	4.1×10^{0}	2.0×10^{0}
CRT	Cerrita	15.092	37.774	-2	1.4×10^{1}	5.2×10^{0}	3.5×10^{-1}	2.8×10^{0}	2.0×10^{0}
PDM	Piedimonte	15.177	37.810	-2	6.1×10^{0}	1.3×10^{1}	1.3×10^{-1}	6.6×10^{0}	1.8×10^{0}
FFD	Fiumefreddo	15.215	37.799	-1	1.6×10^{0}	9.6×10^{0}	2.9×10^{-1}	4.9×10^{0}	1.5×10^{0}
CPV	Campovolo	15.228	37.801	-2	9.5×10^{-1}	8.6×10^{0}	3.2×10^{-1}	4.4×10^{0}	1.4×10^{0}
GDN	Giardini	15.250	37.819	-1	4.0×10^{0}	9.8×10^{0}	3.8×10^{-1}	5.0×10^{0}	1.4×10^{0}
TER	T.Ellera	16.548	38.417	3	1.6×10^{-2}	4.0×10^{-4}	3.5×10^{-1}	1.5×10^{-2}	2.4×10^{-2}

Table 1: Field measurements (locations, loadings, and modes) with the computed tephra loadings obtained ~~by mean of~~with the ARPAE database for the explored TGSDs (Fig. 5).

Table 2: Input parameters used within the numerical models

Parameter	Explored Range	
TGSD	Multiple	
Column height	Multiple	
MER	Multiple	
Exit velocity	Multiple	
Initial magma temperature (°K)	1300	
Exit water fraction (wt%)	2.5	
Radial entrainment coefficient (α)	0.05	0.15
Cross-flow entrainment coefficient (β)	0.05	1.00

Table 2: Input parameters used within the FPlume and FALL3D models. Multiple TGSDs are tested as input for the simulations (see Sect. 3.1). The column height, MER, and exit velocity are set as multiple values (see Sect. 3.2). The simulation scheme is presented in Sect. 3.2 and Fig. 7.

Table ~~2~~3: Best simulation characteristics for each weighted Integrated TGSD

Integrated TGSD	Input		Statistical Metric								Output
Combination (in wt%)	α ($\alpha_1 - \alpha_2$)	β	*K*	*k*	$RMSE_1$	$RMSE_2$	$RMSE_3$	*Correlation*	*Bias*	*TTest*	*TEM* ($\times 10^9$ in kg)
Radar TGSD	0.15 – 0.15	1.00	6.97	9.82	0.97	7.71	0.87	-0.2	-0.3	0.1	5.73
20 Field | 80 Radar	0.06 – 0.09	0.72	1.00	4.35	0.84	2.95	0.74	0.8	0.0	1.0	2.84
40 Field | 60 Radar	0.06 – 0.09	0.40	1.02	3.48	0.81	1.61	0.74	0.8	0.0	1.0	1.66
60 Field | 40 Radar	0.06 – 0.09	0.28	1.01	3.08	0.78	1.53	0.77	0.9	0.0	1.0	1.28
65 Field | 35 Radar	0.06 – 0.09	0.26	1.01	3.02	0.77	1.56	0.77	0.9	0.0	1.0	1.22
70 Field | 30 Radar	0.06 – 0.09	0.25	0.98	2.98	0.77	1.67	0.80	0.9	0.0	1.0	1.21
75 Field | 25 Radar	0.06 – 0.09	0.22	1.02	2.95	0.76	1.64	0.79	0.9	0.0	1.0	1.13
80 Field | 20 Radar	0.06 – 0.09	0.22	0.99	2.96	0.75	1.77	0.82	0.9	0.0	1.0	1.13
85 Field | 15 Radar	0.06 – 0.09	0.21	1.01	3.00	0.75	1.85	0.84	0.9	0.0	1.0	1.10
90 Field | 10 Radar	0.06 – 0.09	0.21	1.00	3.13	0.74	2.02	0.88	0.9	0.0	1.0	1.12
Field TGSD	0.06 – 0.09	0.35	0.99	6.56	0.83	3.65	1.44	0.9	0.0	1.0	1.60

Table ~~2~~3: Statistical metric for the best simulations (i.e. calibration of α and β) for each weighting average combination tested during the inversion of the Integrated TGSD. α is described through α_1 and α_2 within the calculation (Folch et al., 2016). ~~and~~ TEM ~~results~~ indicates the associated theoretical value for each combination~~related to the explored weighting factors used for assessing the Integrated TGSD (i.e. Field + Radar data)~~.

Appendix

Appendix completes Table 2 in terms of parameterizations (i.e. parameters and models) used to run the simulations under the ARPAE and ERA-Interim meteorological databases.

Parameterization	ARPAE	ERA-Interim
Vent elevation (m a.s.l.)	3300	3300
Vent longitude (°Deg)	15.002012	15.002012
Vent latitude (°Deg)	37.746548	37.746548
Time step meteo data (min)	30	30
Longitude nodes	160	115
Latitude nodes	100	100
Grid resolution (km^2)	1	5
Altitude layers (from 0 m a.s.l., 500 m step)	12000	12000
Eruption column model	FPlume [a]	FPlume [a]
Terminal velocity model	Ganser [b]	Ganser [b]
Vertical turbulence model	Similarity [c]	Similarity [c]
Horizontal turbulence model	CMAQ [d]	CMAQ [d]
Gravity current	Yes [e]	Yes [e]

[a] The eruption column model uses the buoyant plume theory (Folch et al., 2016).

[b] The terminal settling velocity is calculated through the Ganser model (Ganser, 1993).

[c] The vertical component of the eddy diffusivity tensor (K_z) is estimated using the similarity option (Costa et al., 2006; Ulke, 2000).

[d] The horizontal component of the eddy diffusivity tensor (K_h) is evaluated as in Byun and Schere (2006) by the CMAQ option.

[e] The gravity current effects in the umbrella region are negligible in the far-field region, but were considered in the simulations (Costa et al., 2013; Suzuki and Koyaguchi, 2009).

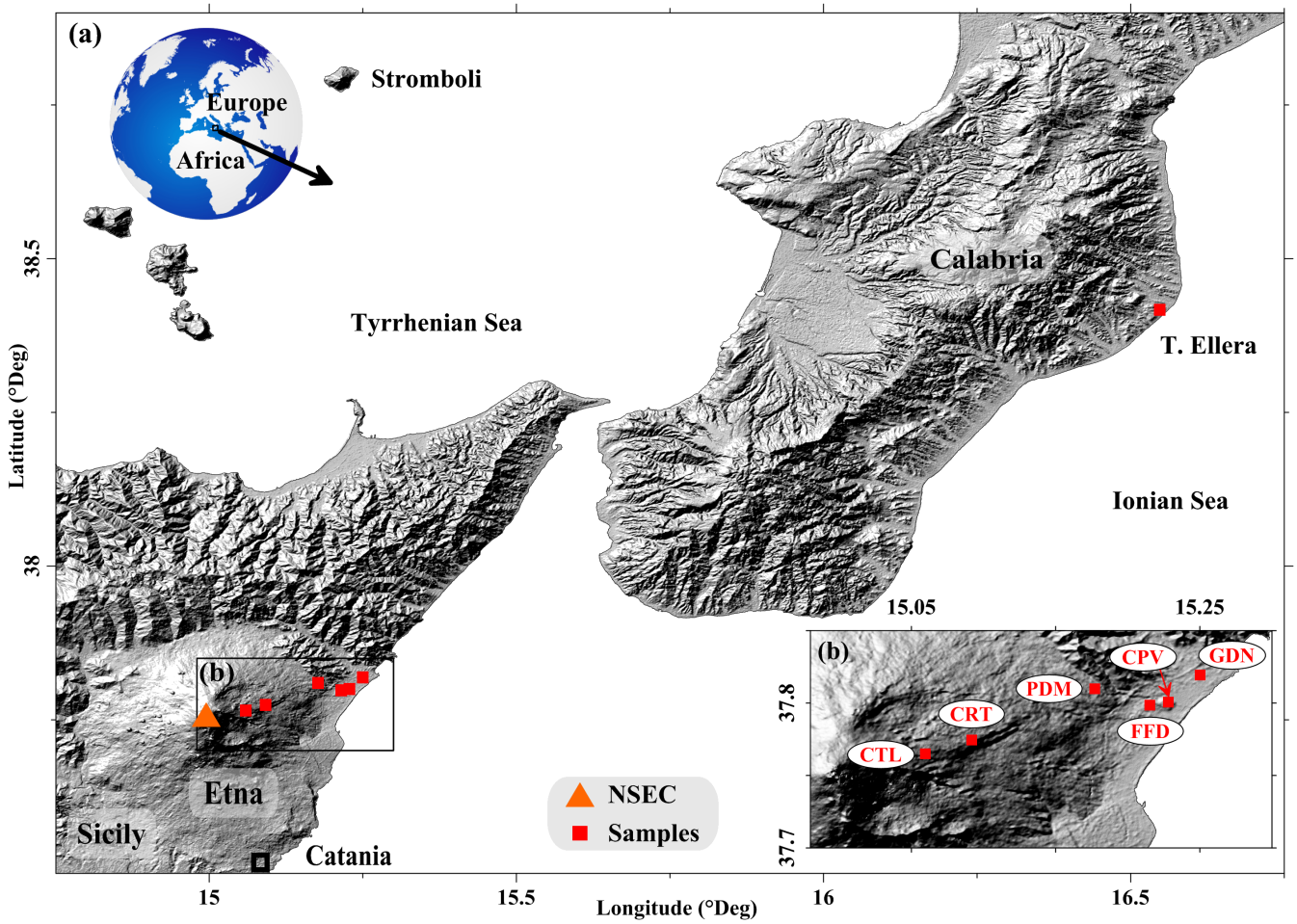

Figure 1: Tephra sample locations (Sicily and Calabria regions, Italy). a) shows the local to medial areas (up to ~160 km from NSEC) affected by the fallout. b) is a zoom indicating the proximal zone (up to ~25 km from NSEC) and the dispersion of the samples. Details in Table 1.

Figure 2: Photograph of the eruption showing the formation of the two volcanic clouds rising at different altitudes (whitish above the brownish). Source: Courtesy of Boris Behncke (INGV–OE).

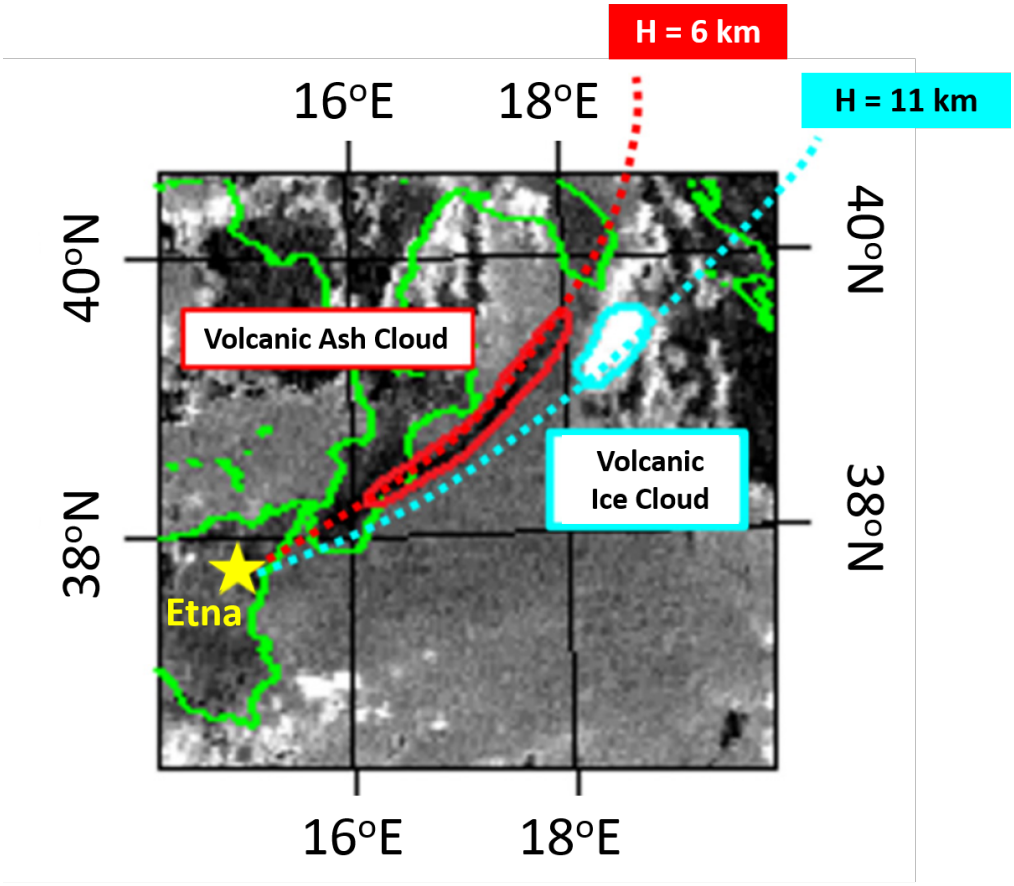

Figure 3: Satellite image (SEVIRI) showing the trajectories of the two volcanic clouds (modified from Figure 17 in Corradini et al., 2016). The ash cloud dispersed towards the Puglia region (southern Italy) at ~6 km a.s.l., whereas the ice/gas cloud moved over Albania at ~11 km a.s.l..

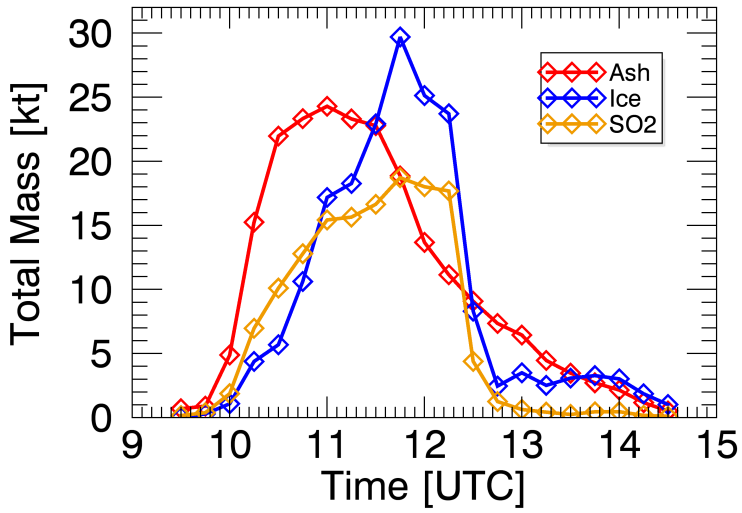

Figure 4: Ash, Ice and SO_2 masses time-series retrieved from SEVIRI for the 23rd November 2013 Etna eruption.

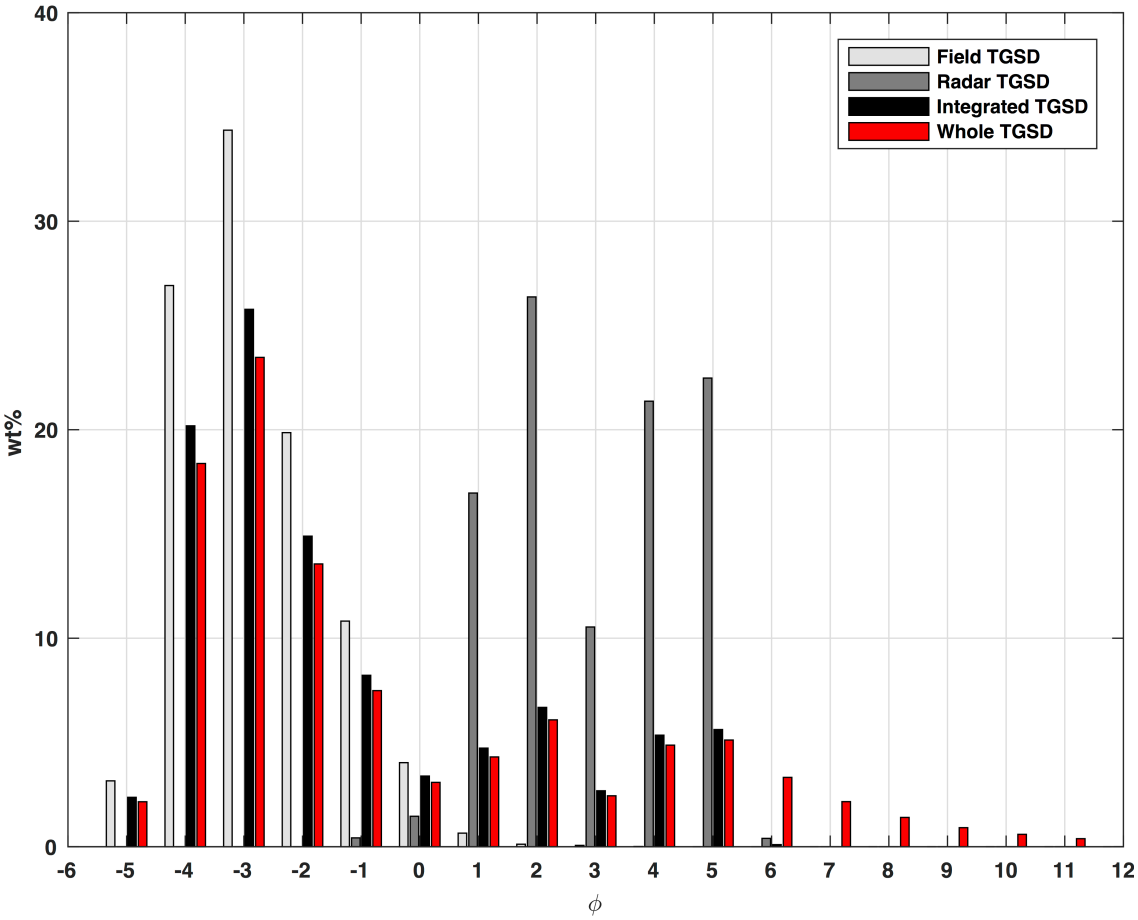

Figure 5: Input TGSDs estimated from either field or X-Radar data. The Integrated TGSD emerges from a weighting average combination of the Field and Radar TGSDs. The Whole TGSD derives from the Integrated TGSD modified to implement the satellite measurements.

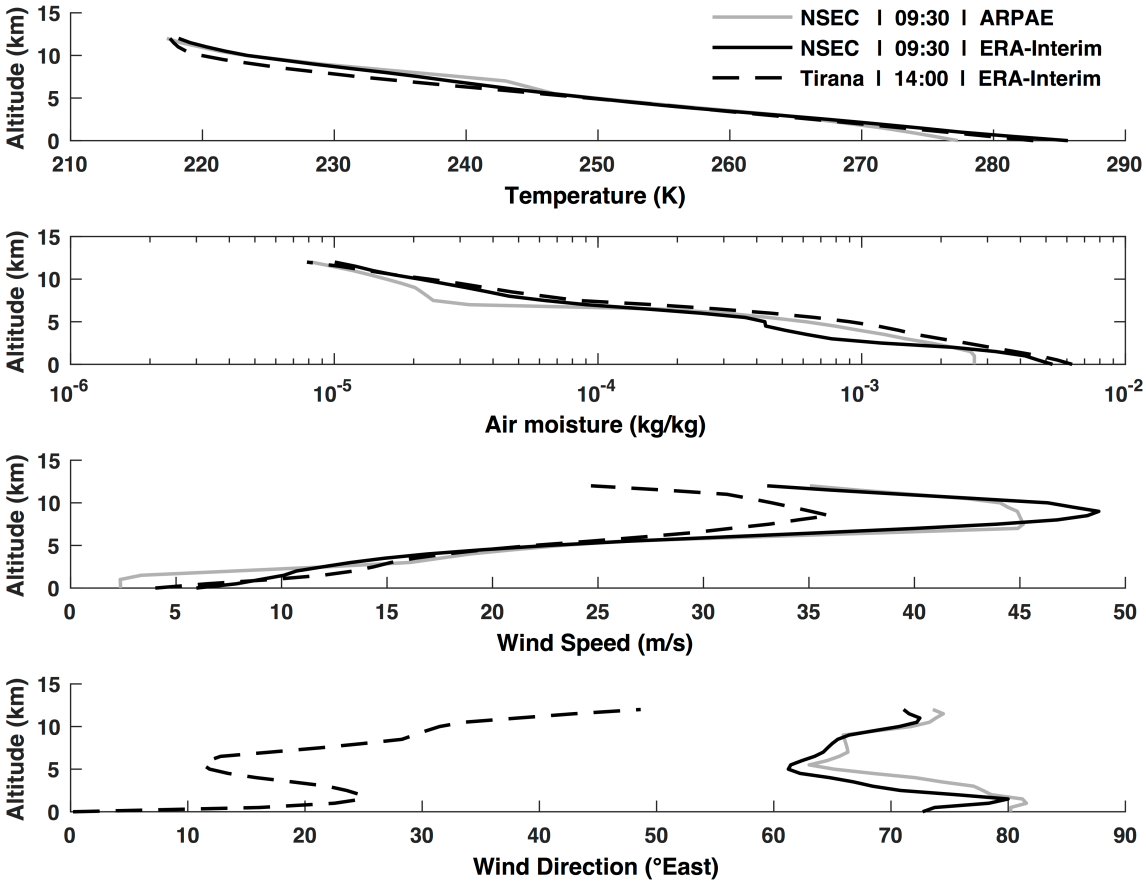

Figure 6: Main meteorological ~~fields~~ profiles ~~represented~~ over ~~the~~ NSEC from ~~the~~ ARPAE (INGV-OE) and ~~the ECMWF (~~ERA-Interim ~~Reanalysis)~~ (ECMWF), ~~platforms~~ and over Tirana city for ERA-Interim.

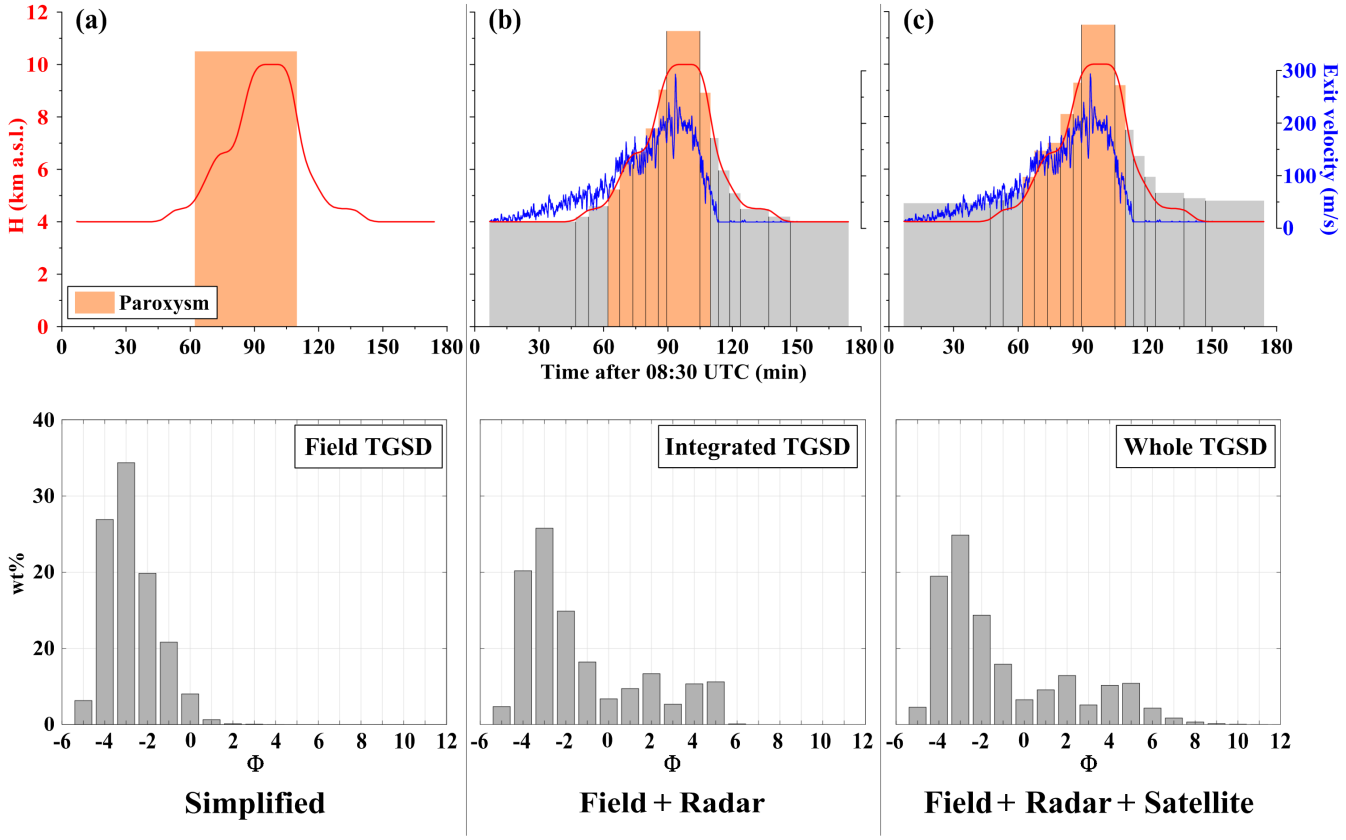

Figure 7: Simulation schemes. a) Simplified procedure. b) discretization of the eruption into a set of phases to account for the temporal variation of the intensity (i.e. column height, hence MER, and exit velocity). The improved scheme is accompanied with ~~Use of~~ **the Integrated TGSD** ~~(field + X-Radar observations) with~~ and ~~the~~ **ARPAE** ~~meteorological~~ **database** ~~and the recorded eruptive column heights and exit velocities~~**. c)** Same procedure as b) ~~Use of~~with **the Whole TGSD** ~~(field + X-Radar + SEVIRI measurements) with~~and **ERA-Interim** ~~database and the recorded eruptive column heights and exit velocities~~**.**

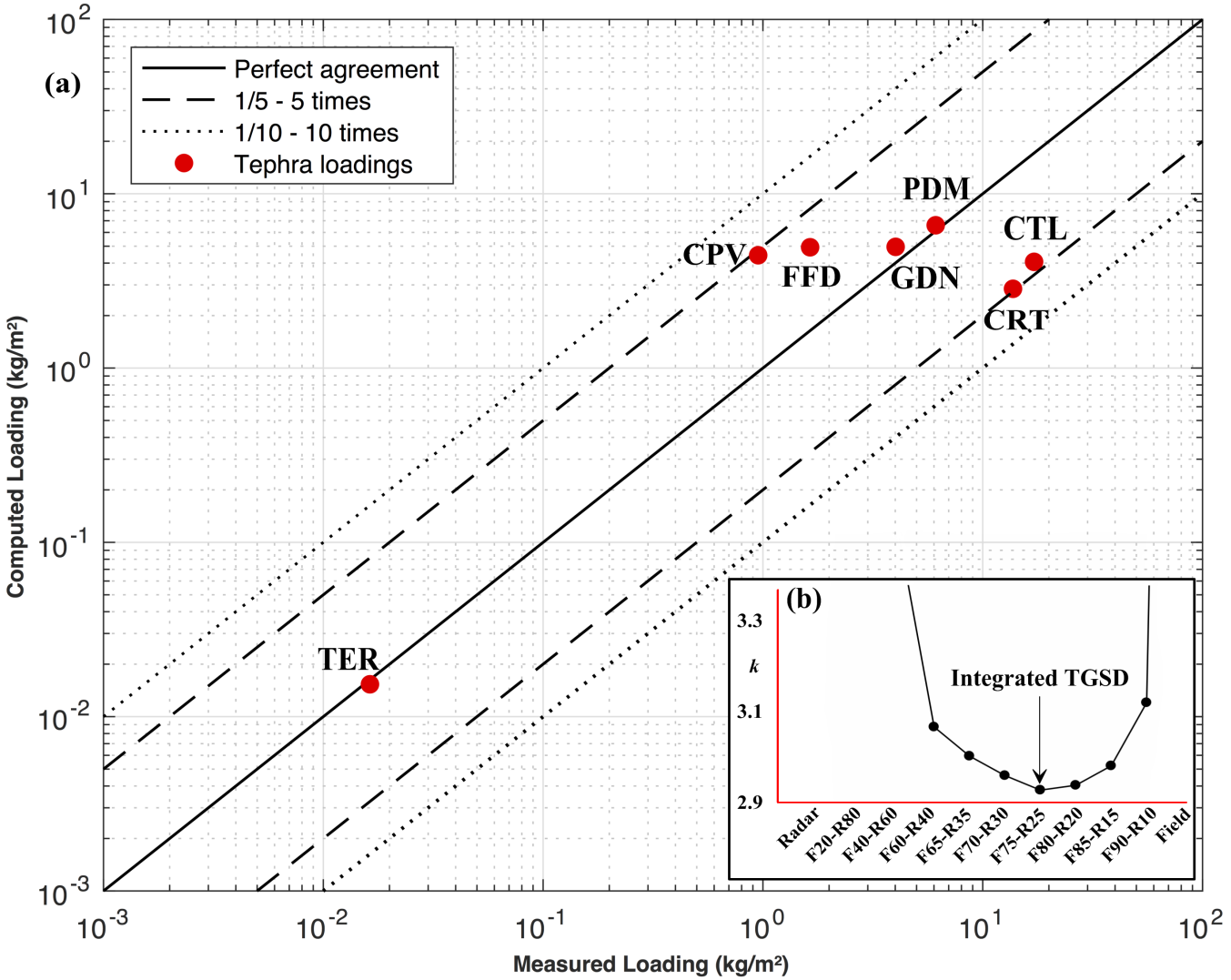

Figure 8: a) Comparative study between the measured and ~~the~~ computed tephra loadings for inverting the Integrated TGSD. b) Graphic of the *k* index showing the optimization for assessing the best weighting averages combination ~~for both the~~to apply to the Field and Radar TGSDs (details in Table 2)

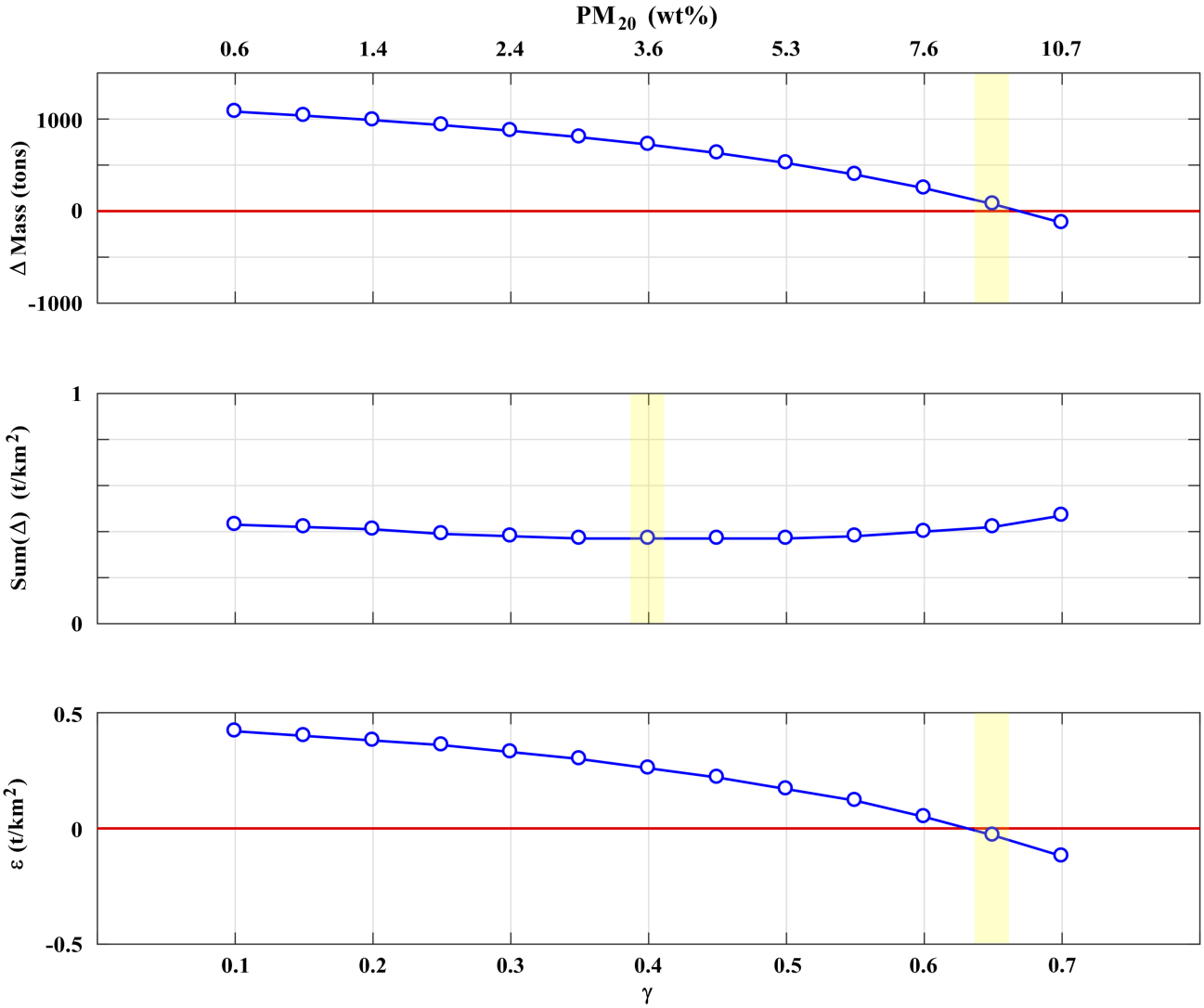

Figure 9: Quantitative analysis of the airborne ash mass measured from SEVIRI and computed by FALL3D to ~~assess~~ invert the PM_{20} fraction ~~of the~~to use within the Whole TGSD ~~necessary~~ for best ~~-~~reproducing the ~~far-travelling tephra~~SEVIRI retrievals. The upper part compares the whole airborne ash masses for the entire eruption, whereas the middle part gives the difference of the absolute average difference of mass per unit area. The lower part quantifies the difference in terms of mass per unit area (details in Sect. 3.3).

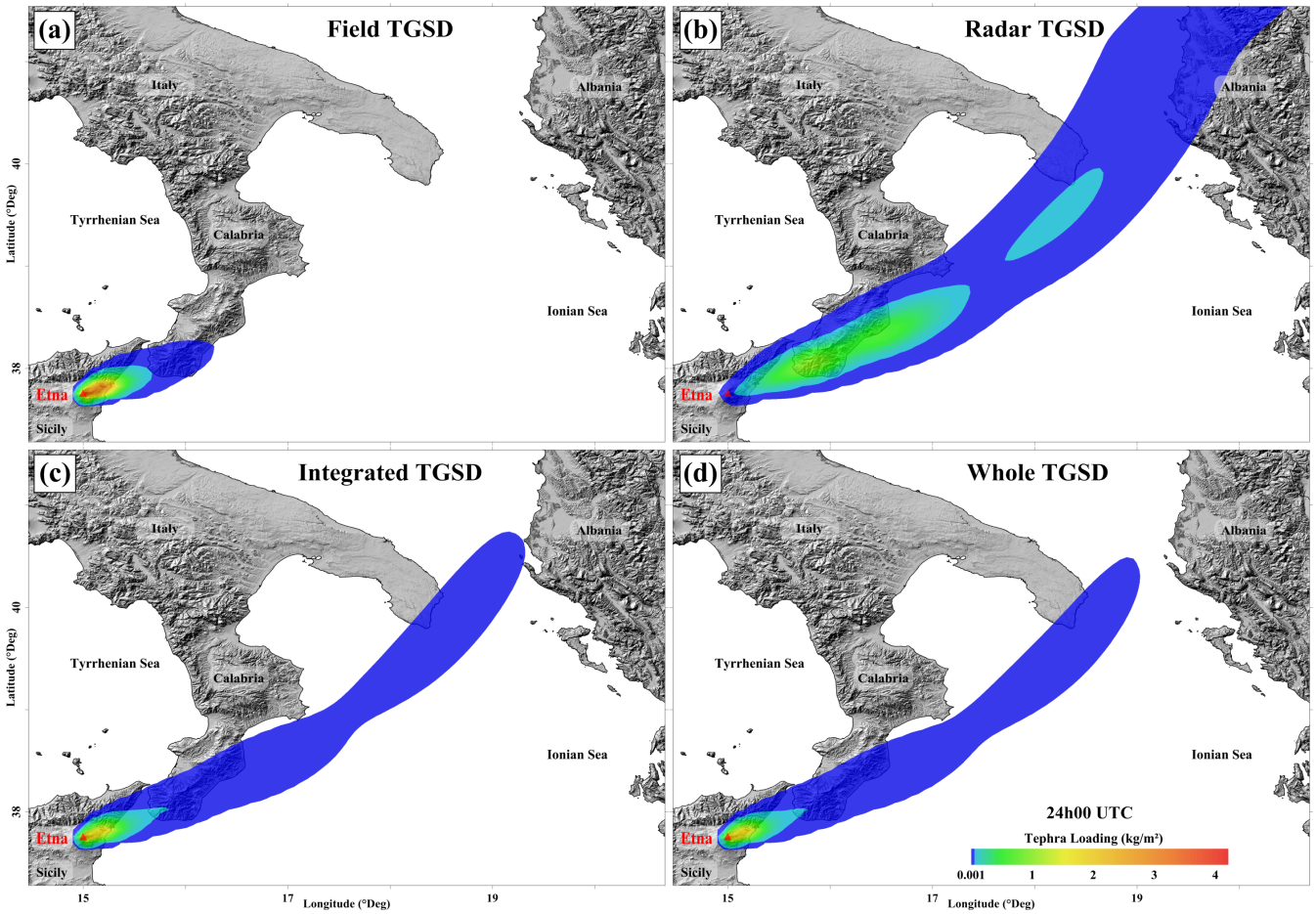

Figure 10: Tephra loading maps computed with the a) Field, b) Radar, c) Integrated, and d) Whole TGSDs, respectively. They indicate the relevance of the integrated approach ~~by validating~~reproducing ~~the tephra fallout expansion and~~ the affected areas.

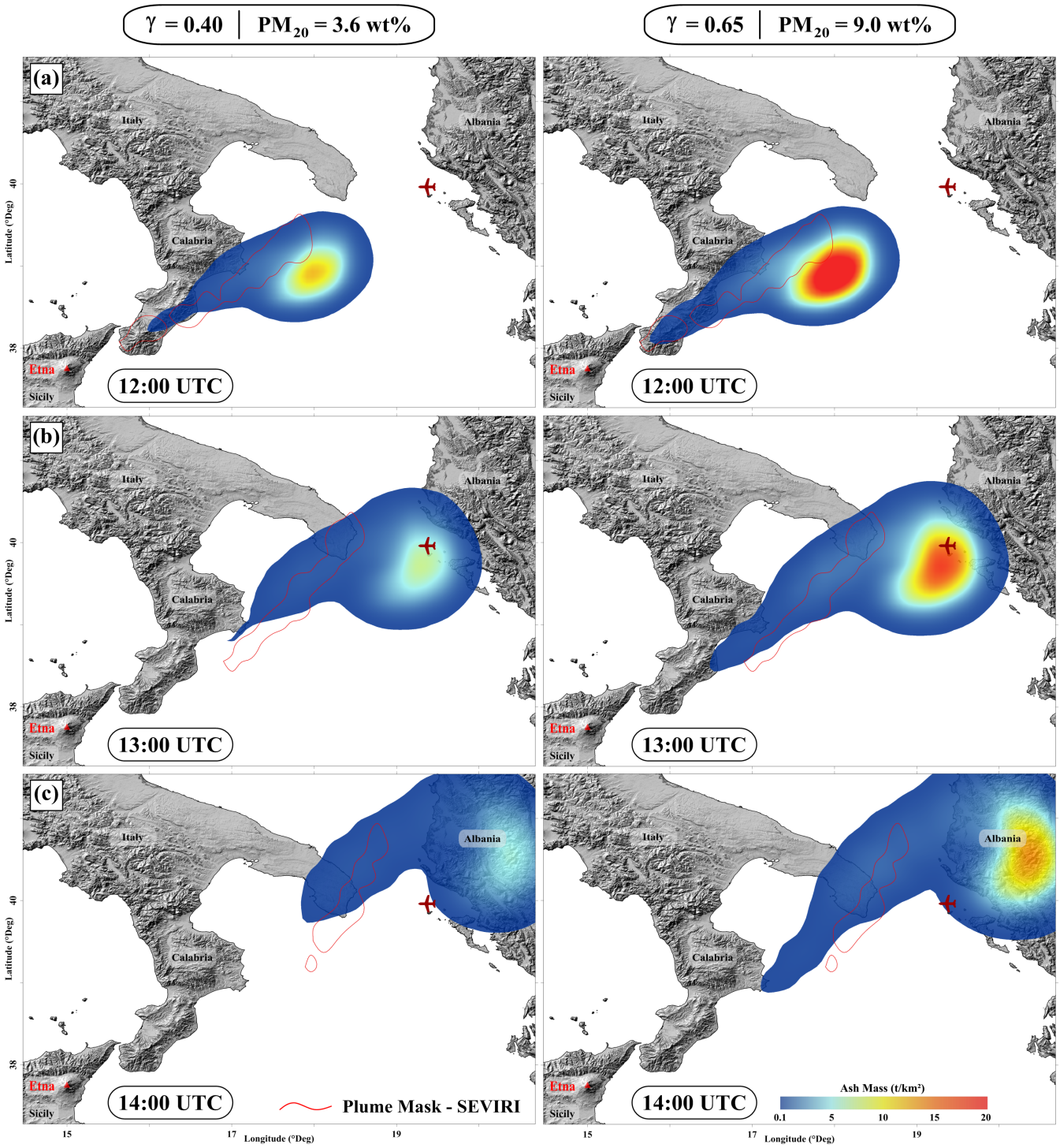

Figure 11: Illustration of the comparative study between the SEVIRI and FALL3D airborne ash masses for a given time (i.e. 12:00, 13:00 and 14:00)~~. The procedure aims at~~to ~~inverting the PM_{20} fraction range to~~ best ~~reproduce~~ reproduce the satellite retrievals ~~(i.e. 3.6-9.0 wt%). The inversion implies the investigation of different γ factor values (associated with a PM_{20} fraction) within the Whole TGSD~~.